Single cell RNA-seq reveals changes in cell cycle and differentiation programs upon aging of hematopoietic stem cells

Monika S. Kowalczyk[1,†], Itay Tirosh[1,†], Dirk Heckl[2], Tata Nageswara Rao[3,4], Atray Dixit[1], Brian J. Haas[1], Rebekka K. Schneider[2], Amy J. Wagers[3,4,5,6], Benjamin L. Ebert[2], Aviv Regev[1,6,7,*]

Affiliations

[1] Broad Institute of MIT and Harvard, Cambridge, MA, 02142, USA.

[2] Division of Hematology, Department of Medicine, Brigham and Women's Hospital, Harvard Medical School, Boston, MA, USA.

[3] Harvard Stem Cell Institute and Department of Stem Cell and Regenerative Biology, Harvard University, Cambridge, MA, USA.

[4] Joslin Diabetes Center, Boston, MA 02215, USA.

[5] Paul F. Glenn Laboratories for the Biological Mechanisms of Aging, Harvard Medical School, Boston, MA, USA.

[6] Howard Hughes Medical Institute.

[7] Department of Biology, Massachusetts Institute of Technology, Cambridge, MA, 02140, USA.

* Corresponding author

† These authors contributed equally to this work

Contact Information

Aviv Regev, Broad Institute of MIT and Harvard, 415 Main Street, Cambridge, MA 02142,

aregev@broadinstitute.org

Keywords: single-cell RNA-seq, hematopoiesis

Abstract

Both intrinsic cell state changes and variations in the composition of stem cell populations have been implicated as contributors to aging. We used single cell RNA-seq to dissect variability in hematopoietic stem and progenitor cell populations from young and old mice from two strains. We found that cell cycle dominates the variability within each population, and that there is a lower frequency of cells in the G1 phase among old compared to young long-term hematopoietic stem cells, suggesting that they traverse through G1 faster. Moreover, transcriptional changes in HSCs during aging are inversely related to those upon HSC differentiation, such that old short term (ST)-HSCs resemble young long-term (LT-HSCs), suggesting that they exist in a less differentiated state. Our results indicate both compositional changes and intrinsic, population-wide changes with age and are consistent with a model where a relationship between cell-cycle progression and self-renewal versus differentiation of HSCs is affected by aging and may contribute to the functional decline of old HSCs.

Introduction

A rare population of multipotent hematopoietic stem cells (HSCs) is required for the continuous production of millions of mature blood cells, while maintaining a correct balance between the different lineages. At the apex of the hematopoietic hierarchy reside the most primitive long-term reconstituting HSCs (LT-HSCs). LT-HSCs can undergo three types of cell division: (**1**) a renewal symmetric cell division to produce two LT-HSC daughter cells that replenish the LT-HSC pool; (**2**) a commitment symmetric division to replenish committed cells producing short-term reconstituting HSCs (ST-HSCs) and subsequently multipotent progenitors (MPPs); and (**3**) asymmetric division, where one daughter cell remains a stem cell, while the other becomes committed.

This remarkable capacity of HSCs declines with age as reflected by an accumulation of HSCs in the bone marrow (Morrison et al. 1996; de Haan et al. 1997; Sudo et al. 2000; Rossi et al. 2005) that show decreased regenerative potential (Morrison et al. 1996; Sudo et al. 2000; Kim et al. 2003; Rossi et al. 2005; Dykstra et al. 2011), and a myeloid-skewed differentiation potential (Sudo et al. 2000; Kim et al. 2003; Liang et al. 2005; Rossi et al. 2005). Relatedly, in the elderly, there is an increased incidence of myeloid diseases, such as leukemias (Lichtman and Rowe 2004), a decreased competence of the adaptive immune system (Linton and Dorshkind 2004) and the onset of anemia (Beghe et al. 2004).

Despite extensive studies documenting the decline of HSC function during aging, the molecular mechanisms underlying HSC aging have remained obscure. Current views of stem cell aging converge to two main models: **(1)** clonal selection, implying that multiple HSC clones with specific phenotypes coexist but their relative frequencies change with age; **(2)** a global population shift in intrinsic cell states, in which all HSCs in the population undergo coordinated changes in functional potential with age. Previous transcriptional profiling limited to populations of young and old LT-HSCs demonstrated upregulation of myeloid genes and downregulation of lymphoid and cell cycle genes with age (Rossi et al. 2005; Chambers et al. 2007; Sun et al. 2014). However, such population measurements may obscure

important cell-to-cell variability in gene expression and could not definitively distinguish between these two models, and thus cannot determine whether there are distinct, cell intrinsic, functional states of HSCs that are age-dependent, or whether the observed transcriptional differences between bulk populations reflect changes in the proportions of subgroups of cells.

New advances in single cell genomics (Wills et al. 2013), especially single cell RNA-seq (Hashimshony et al. 2012; Ramskold et al. 2012), have opened the way to characterize distinct functional states of individual cells, even within seemingly homogeneous immune cell populations (Shalek et al. 2013; Mahata et al. 2014; Shalek et al. 2014). These should allow us to distinguish changes that arise from cell-intrinsic differences in transcriptional states from those that reflect changes in the proportion of sub-populations. Furthermore, single cell analysis should allow us to relate prospective profiles of HSCs that have just been isolated with known heterogeneity in their retrospective functional capacity in transplantation assays.

Here, we leveraged single cell RNA-seq to directly assess transcriptional heterogeneity within the HSCs and how it may change with age in the steady-state unperturbed hematopoiesis. Given that HSCs are functionally heterogeneous as revealed through transplantation studies (Dykstra et al. 2007; Challen et al. 2010; Muller-Sieburg et al. 2012), we hypothesized that this retrospective variability (assessed through the outcome of a transplant) would be prospectively reflected in the transcriptional profiles of cells in unperturbed conditions.

Results

Single cell RNA-seq of ~1,200 HSCs

To systematically characterize the global transcriptional landscape of individual cells in the course of the first steps of mouse hematopoiesis we used multiparameter fluorescence-activated cell sorting (FACS) followed by single-cell RNA-seq using SMART-seq, as previously described (Ramskold et al. 2012;

Shalek et al. 2013; Shalek et al. 2014) (**Methods**). We prospectively isolated three cell types using LSK (lineage$^-$, SCA1$^+$, KIT$^+$) and SLAM (Signaling lymphocyte activation molecule) markers whose expression is conserved across mouse strains and during aging (Kiel et al. 2005; Yilmaz et al. 2006): long-term hematopoietic stem cells (LT-HSCs) (LSK CD150$^+$CD48$^-$), short-term hematopoietic stem cells (ST-HSCs) (LSK CD150$^-$CD48$^-$) and multipotent progenitors (MPPs) (LSK CD150$^+$CD48$^+$) from young (2-3 months) and old (>22 months) C57BL/6 mice (**Figure 1A, B and C**). Consistent with previous work (Morrison et al. 1996; de Haan et al. 1997; Sudo et al. 2000; Rossi et al. 2005), we observed a significant expansion of LT-HSCs with age (~6-fold, $p<0.001$) in total bone marrow (**Figure 1D**) and in the stem cell compartment (**Figure 1E**). In contrast, ST-HSCs frequency within the LSK compartment of old mice was comparable and MPP frequency decreased, possibly indicating an imbalance between self-renewal and differentiation.

We generated 1,152 single cell RNA-seq profiles, along with corresponding population controls, from six populations: three cell types (LT-HSCs, ST-HSCs, and MPPs) at each of the two ages (2-3 months and >22 months; nearly 200 cells per cell type and age). Our stringent filtering criteria retained 1,059 high quality libraries for subsequent analyses (~176 per cell type and age on average; see **Methods** for QC details and filtering criteria). Aggregated *in silico*, the average single cell gene expression profile of the individual cells from a given cell type reproduced the gene expression profile of its matching population control (r~0.9 on average) (**Figure 1F and G**). Additionally, profiles of populations or aggregated single cells were highly correlated between young and old mice, indicating that aging-related differences may be subtle (**Figure 1G**). Finally, the RNA expression levels of markers used for sorting these cell types or known to correlate with them reproduced known associations (**Figure 1H**).

Cell cycle is a main source of transcriptional variation between HSCs

To uncover the main sources of variation, we performed principal component analyses (PCA) for each cell type and age separately. Strikingly, in every case, the top principle components (PCs) were associated

primarily with cell cycle-related genes (**Figure 2A**), indicating that transcriptome heterogeneity here is dominated by cell cycle status. Furthermore, analysis of known mouse hematopoietic transcriptional modules (Jojic et al. 2013; Shay et al. 2013) showed strong co-regulation across single cells only for genes in cell cycle modules (**Figure S1A**). When we analyzed only those cells without appreciable expression of cell cycle genes (65% of all cells), the highest remaining co-regulation was for a ribosome module, with an average correlation lower than 0.1 in each of the six populations (**Figure S1B**). We thus concluded that cell cycle reflects the main source of heterogeneity within the transcriptomes of each HSC cell type and age.

To further dissect the cell cycle states we scored each cell for its likely cell cycle phase using signatures for the G1/S, S, G2, and G2/M phases defined based on functional annotations (Reference Genome Group of the Gene Ontology 2009) and profiles from synchronized HeLa cells (Whitfield et al. 2002) and further refined by co-expression in our profiles (**Methods**). To directly confirm that these signatures correspond to different cell cycle phases, we separated cell cycle phases of KIT enriched cells by concurrent Pyronin Y and Hoechst staining (**Figure 2B**). RNA sequenced from 11 gates representing the cell cycle continuum showed precise partitioning based on our signatures as expected (**Figure 2C**). Lastly, we confirmed that these signatures robustly detect cell cycle phases in other single cell datasets from human and mouse (Macosko et al. 2015) (**Figure S2**).

Clustering all HSCs by the expression of these signatures uncovered three distinct groups of cells: cluster 1 that expresses primarily G2/M phase genes (*e.g.*, mitosis genes), cluster 2 with high expression of G1/S phase genes (*e.g.*, DNA replication genes) and cluster 3 that does not show expression of cell cycle genes (non-cycling or quiescent cells) (**Figure 2D** and **S3B**). The frequency of cells in the G1/S and G2/M clusters (cycling cells) was considerably higher in MPPs than in LT- and ST-HSCs (**Figure 2E** and **Figure S3C-E**), consistent with the known high level of proliferation of MPPs (Wilson et al. 2008).

Almost a third of the analyzed genes (2,708 genes, ~32%) were found to have significant cell cycle-dependent expression changes that were consistent among multiple HSC cell types or ages (**Figure S4A, Table S1**). The vast majority of cell cycle regulated genes (92%) were upregulated in cycling *vs*. non-cycling cells (see **Table S1** for phase-specific upregulation); the minority of cell-cycle regulated genes (8%) that were upregulated in non-cycling *vs*. cycling cells included several transcription factors that could be important for regulating HSC quiescence (*e.g.*, *Stat1*, *Stat3*, *Meis1*, *Pbx1*, *Klf6*, *Nfia*; **Table S1**).

A G1-specific depletion in old LT-HSCs

Age did not typically affect the proportion of cells within each cluster, with one notable exception of old LT-HSCs, where the frequency of cells in cluster 1 (G1/S cluster) was significantly decreased in old *vs.* young cells (7.6% *vs.* 22%, *P*=0.0023; hypergeometric test, **Figure 2E** and **Figure S3E**). The depletion of cells in the G1/S phases was specific to old LT-HSCs, and was not observed for either old ST-HSCs or MPPs. We confirmed a decrease in the frequency of old LT-HSCs that are in the G1 phase by an orthogonal approach of staining bone marrow cells with Ki67/Hoechst paired with BrdU incorporation followed by FACS (~2-3 fold decrease, p=0.012 independent samples *t*-test, **Figure 2G** and **H**) with similar proliferation rates by *in vivo* BrdU incorporation (mean 19.6% and 20.1% for old and young respectively, p=0.916 independent samples *t*-test, **Figure 2I and J**).

A decreased proportion of cells observed in specific cell cycle phases (G1/S here) suggest more rapid transitions through these phases (Kafri et al. 2013), implying a shorter G1 and/or S phases. Multiple studies, in mouse and human cells, established that G1 length varies widely among different cell types, is short specifically in self-renewing cells, and increases with differentiation (Li et al. 2012; Coronado et al. 2013). We thus reasoned that the same trend may hold in LT-HSCs, where aging could be accompanied by a decrease in G1 length and LT-HSC accumulation.

To refine our hypothesis of a G1-specific depletion in old LT-HSC, we performed a higher-resolution analysis of cell cycle progression using our single cell profiles. Plotting the average expression of G1/S *vs*. G2/M genes in each cell revealed a complete cell cycle trajectory (**Figure 2F**). Using the location of cells on that trajectory we ranked cells with respect to their cell cycle progression (Kafri et al. 2013; Trapnell et al. 2014). We roughly estimated the range of cell ranks that might correspond to distinct phases of the cell cycle, with ~20%, 6%, and 9% of cells in G1, S and G2/M, respectively, and 65% of cells in the G0 non-cycling state (**Figure S4B, Table S2**). Comparing the frequencies of old to young LT-HSC along the cell cycle progression ranks revealed the most pronounced depletion within the late G1 phase (~4-fold; **Figure S4C-E**). To confirm this finding, we isolated and sequenced an additional 200 single cells of LT-HSCs and of ST-HSCs, from an additional set of old C57BL/6 mice. Once again, we observed a significant age-dependent decrease in the frequency of cells in G1 phase among LT-HSCs, but not ST-HSCs (**Figure S4D**). Taken together, our experiments and analyses all support the finding that old LT-HSCs specifically have a smaller pool of cells in the G1 phase.

G1 phase is a sensitive period during which cell fate decisions are made (Takahashi et al. 1995; Sherr 2000; Calegari and Huttner 2003; Massague 2004; Pauklin and Vallier 2013). Furthermore, mouse embryonic stem cells continue to self-renew and thus avoid differentiation by eliminating or greatly shortening their early G1 phase (Savatier et al. 1994; White et al. 2005). Recent work has also demonstrated that unlike the majority of slow-cycling cells with stochastic and inefficient reprogramming to pluripotency, a small subset of hematopoietic cells with rapid G1 can be deterministically reprogrammed, raising the possibility that G1 length may be linked to dedifferentiation (Guo et al. 2014). We therefore speculated that a short G1 in old LT-HSCs might be linked to a dedifferentiated state. This hypothesis is also consistent with recent epigenomic analyses of young and old HSCs (Sun et al. 2014).

Opposing transcriptional states for aging and differentiation in HSCs

To test for a possible link between HSC aging and self-renewal/differentiation, we first excluded the 367

cycling cells (to avoid the dominant effects of the cell cycle) and performed a joint PCA on the remaining 692 non-cycling cells (contains all cell types and ages). Each of the first two PCs segregated HSCs by cell type and age (**Figure 3A-E,** see **Figure S5A** for additional PCs). Accordingly, with respect to these two PCs, young LT-HSCs are clearly distinct from the old LT-HSCs (due to an age effect; **Figure 3B** and **E**; the same plot as in **Figure 3A**, but only specific pairs of populations that differ by age are displayed), as well as from the young ST-HSCs (due to a differentiation effect; **Figure 3C** and **E**; the same plot as in **Figure 3A**, but only specific pairs of populations that differ by differentiation are displayed). Interestingly, young LT-HSCs are similar to the old ST-HSCs that differ in both age and differentiation state (**Figure 3D** and **E**). Consistently, both PC1 and PC2 were inversely associated with differentiation and aging, scoring high both for cells from younger animals (**Figure 3A** and **B**) and from more differentiated cells (**Figure 3A** and **C**; *e.g.*, MPPs and ST-HSCs from either young or old mice score higher than their age-matched LT-HSC counterparts) and scoring low both for old cells and for less-differentiated cells. These results were reproduced also with the expression profiles from the replicate experiment (~200 LT-HSCs and ~200 ST-HSCs; different mice obtained, sorted and profiled months apart) (**Figure S5B**). Thus, the transcriptional program of old LT-HSCs and ST-HSCs resemble a less differentiated state than their young counterparts, which could reflect loss of balance between self-renewal and differentiation. This could be linked to the recent finding of a developmental switch, where in embryonic development LT-HSCs are the main contributors for most blood-cell production in unperturbed hematopoiesis, while in adult life ST-HSCs assume that role (Busch et al. 2015). To investigate the clonogenic potential of individual LT-HSC and ST-HSCs from young and old mice regardless of their reconstituting activity *in vivo*, we assessed colony formation on methylcellulose. While young LT- and ST-HSCs gave rise to similar number of colonies, both old counterparts formed significantly more colonies (1.4 and 1.3 increase in LT- ($p<0.001$) and ST-HSC ($p=0.01$) respectively, independent samples *t*-test, **Figure 3F**).

Notably, PC1 and PC2 also correlate with an expression signature of megakaryocyte progenitors (MkP) (as defined in (Sanjuan-Pla et al. 2013); **Figure 3F; see Figure S4C** for other signatures), such that old cells express, on average, higher levels of MkP signature genes than their young counterparts and less-differentiated cells have higher MkP expression levels than more differentiated cells (**Figure 3F**) ($P<10^{-6}$ for all pairwise comparisons by Mann-Whitney *U* test). This is largely consistent with the reported myeloid bias of old HSCs (Rossi et al. 2005), but MkP signature genes, and more generally, myeloid-related genes appear to account for only a minority of a larger expression program that is altered during HSC differentiation and aging. For example, the 792 genes that are enriched in at least one of four myeloid progenitor cell types (MkP, pre-CFU, preMegE, preGM) (Sanjuan-Pla et al. 2013) include only 24 of the top 100 genes that correlate negatively with PC1+PC2 and therefore increase with age, and only 16 of the top 100 genes that correlate positively with PC1+PC2.

To identify candidate genes that may underlie this inverse relationship, we compared the expression of each gene between pairs of populations that differed by differentiation (LT-HSCs *vs*. ST-HSCs) or by age (young *vs*. old), but were matched for the other parameter. Overall, we performed three comparisons for the effects of differentiation (LT- *vs*. ST-HSCs in young mice and in two replicates of old mice) and four comparisons for the effects of aging (young *vs*. old LT- and ST-HSCs, each with two replicates) to first identify significant differences ($p<0.05$, two-sample *t*-test, no correction for multiple tests) between each pair of conditions. We then identified 78 genes with a consistent aging and differentiation effect (FDR<0.05, **Methods, Table S3**). Of these, all but one gene (*Ctnnal1*) showed an opposite trend with aging and differentiation, suggesting an inverse relationship between these variables (**Figure 4A and B**). This list of genes includes several important regulators of hematopoiesis and/or self-renewal, such as *Flt3*, *Cd34, Vwf, Il16, Nfia*, *Id2*, *Itgb3, Runx1t1,* and *Cd44* (**Figure 4A**). Expression changes for some of these genes were consistent with a potential imbalance between self-renewal and differentiation or a defect in the differentiation of old LT-HSCs, as *Flt3* and *Cd34* (lowest in old LT-HSCs) have previously been

linked to HSC differentiation. We further validated at the protein level that CD34 and FLT3 decrease with aging and increase with differentiation (**Figure 4C**).

An age-independent expression program among MPPs but not other cell types

While the aging-differentiation expression program described above appears to dominate the variability among all non-cycling HSCs (*i.e.* from the three cell types together), we next asked whether we could identify additional sources of variability within each individual cell type. PCA performed independently on the non-cycling LT-HSCs (**Figure 5A**) and ST-HSCs (**Figure 5B**) (as opposed to a joint PCA for all cells and ages in **Figure 3**) showed that aging dominates the cell-to-cell variability within both of these cell types and we could not find additional major independent sources of variability, such as additional subsets of cells. This suggests that most variation discernible within LT-HSCs or ST-HSCs and not related to cell cycle status, is associated with cell-intrinsic changes that manifest rather uniformly across each population, rather than with the emergence of specific subsets. We discuss how this relates to known functional heterogeneity below (see **Discussion**).

In contrast, among non-cycling MPPs we found that expression variability is largely independent of age (**Figure 5C**), and detected an age-independent expression program whose levels vary considerably within the immunophenotypically defined MPP compartment (**Figure 5D**). This uncovered two cell states within MPPs, which have discrete molecular signatures: gene-set1 and gene-set2 (**Figure 5D**; **Table S4**), yet representing part of a continuous spectrum, irrespective of age (**Figure 5E**). Enrichment analysis using gene sets from lineage-restricted progenitors (Pronk et al. 2007; Sanjuan-Pla et al. 2013) revealed a lymphoid bias for gene-set1 and pre-megakaryocyte/erythroid and megakaryocyte progenitor bias for gene-set2 (**Figure 5F**). This highlights MPPs as a heterogeneous population likely including both lymphoid-biased and myelo-erythroid-biased progenitors, in line with MPPs giving lymphoid and myelo-erythoird reconstitution in competitive transplants (Oguro et al. 2013).

Age-associated changes are conserved between mouse strains

Life span and aging vary between mouse strains. For example, C57BL/6 mice are long-lived compared to the short-lived DBA/2 mice (Turturro et al. 1999). To test the generality of our observations, we also examined LT-HSCs, ST-HSC and MPPs in young and old mice from the DBA/2 strain, which originates from a distinct breeding lineage (Fox 1997).

Using Slam markers with conserved expression among mouse strains (Kiel et al. 2005) and ages (Yilmaz et al. 2006) (**Figure 6A, S6A and B**) we quantified the frequency of LT-HSCs, ST-HSC and MPPs in bone marrow by flow cytometry (**Figure 6B**) and stem cell compartment (LSK) of young and old DBA/2 mice (**Figure S6C**). We observed an age-associated increase of LT-HSCs frequency, albeit to a lower extent (~2-fold, $p<0.001$) than in C57BL/6 (~6-fold, $p<0.001$) (**Figure 6B**). Moreover, hemoglobin concentration and red blood cell (RBC) numbers were significantly lower in aged mice (hemoglobin 10.3 *vs* 12.7 g/dl, p=0.001 and RBC 8.2 *vs* $9.2*10^6$/µl, $p=0.04$, independent samples *t*-test), indicating anemia, than in C56BL/6 mice (hemoglobin 11.8 *vs* 14g/dl, $p=0.001$ and RBC 8.38 *vs* $9.9*10^6$/µl, $p<0.001$).

Next, we used two approaches to compare the cell cycle distribution between young and old LT-HSCs from DBA/2 mice. First, we performed single cell RNA-seq with prospectively isolated LT-HSC, ST-HSCs and MPP from young and old DBA/2 mice. Our high-resolution cell cycle analysis again revealed the entire cell cycle trajectory (**Figure 6C**) and a modest (~2-fold) depletion of old LT-HSCs in a region of the cell cycle trajectory that presumably reflects the early G1 phase (**Figure 6E**). Second, staining bone marrow with Ki67/Hoechst showed a decrease in the frequency of old LT-HSCs that are in the G1 phase (**Figure 6D and S6D**). FACS analysis showed a similar, albeit non-significant, trend for ST-HSCs (**Figure S6D**). Taken together, a specific depletion of old LT-HSCs in the G1 phase appears to be conserved between C57BL/6 and DBA/2 strains.

Finally, we examined the conservation of the expression programs described above. PCA of all non-cycling DBA/2 cells recapitulated the results in C57BL/6 and showed that the first two PCs are negatively associated with age (**Figure S6E** and **F**) and positively associated with differentiation (*i.e.* ST-HSCs *vs.* LT-HSCs) (**Figure S6E** and **G**). As in C57BL/6, young LT-HSCs are more similar to old ST-HSCs than to old LT-HSCs in DBA/2 (**Figure S6H**). Moreover, while the genes associated with PC1 and PC2 partially differ between the two strains, using the top genes that discriminate age and differentiation states in C57BL/6 as a signature, we recapitulated the same effect in DBA/2 (**Figure 6F**). As in C57BL/6, PCA among non-cycling cells within each cell type showed the dominant effect of age for LT-HSCs and ST-HSCs, but not for MPPs (**Figure S7A-C**). MPPs showed a similar pattern as in C57BL/6, where two cell states, one lymphoid-biased and the other myeloid-biased (**Figure S7G**), co-exists within the phenotypically defined MPPs (**Figure S7D** and **E**). Taken together, all of our main results in C57BL/6 are largely recapitulated in DBA/2, further strengthening their generality.

Discussion

Cellular heterogeneity of young HSCs

Despite markers that can give high levels of HSC purity, HSC populations remain functionally heterogeneous both with respect to their self-renewal potential upon transplantation (Benveniste et al. 2010; Morita et al. 2010) and in the ratio of myeloid to lymphoid cells that they generate upon transplantation into irradiated mice (Muller-Sieburg et al. 2002; Dykstra et al. 2007; Kent et al. 2009; Beerman et al. 2010; Challen et al. 2010; Morita et al. 2010). Here, we examined if this retrospective heterogeneity would be prospectively reflected in the transcriptional profiles of single cells. To approach this question, we profiled, for the first time, a very large number of extremely rare single cells from three different cell types (LT-, ST-HSCs & MPPs), two ages (young and old) and two strains (C57BL/6 & DBA/2) using single-cell RNA-seq. This allowed us to assess the current or prospective view of potential HSC attributes through a direct approach of surveying the current transcriptional state of individual cells in steady-state unperturbed hematopoiesis, to complement retrospective analysis by transplantation (perturbed hematopoiesis).

We identified extensive transcriptome variability among HSCs, and associated it to the cell cycle, differentiation, and age. After accounting for these sources of variability, we do not observe discrete subsets of cells within LT-HSCs and ST-HSCs from either age or strain of mice. We relied on a SLAM markers sorting strategy, one of the best strategies to enhance HSC purity, as 47% of single LSK CD150+CD48- bone marrow cells (1 in 2.1) give long-term multilineage reconstitution (Kiel et al. 2005). Similarly, previously observed patterns of long-term repopulation (α, β, δ, γ)although sorted using a different strategy (isolated from $CD45^{mid}lin^{-}Rho^{-}SP$) occur in high frequencies 27%, 39%, 22% and 12% for α, β, δ and γ cells respectively (Dykstra et al. 2007). These proportions are sufficiently high to ensure that if these 47% of LT-HSC SLAM cells or α, β, δ and γ cells have a transcriptional profile or signature that prospectively (prior to transplantation) distinguishes them from other cells they will be readily

discernible in the ~600 LT-HSCs we have analyzed. Surprisingly, that has not been the case. While we have not seen a discernible profile that characterizes a distinct subset of LT- (or ST-) HSCs, our computational methods readily discern subpopulations within MPPs (which may indicate an initial specification of HSCs into myeloerythroid and lymphoid lineages); thus, the lack of detectable HSC transcriptional subpopulations, within a given cell type and age, is likely not due to a simple weakness in computational methods. In particular, we extensively searched for recently reported platelet-biased LT-HSCs within our single-cell dataset using previously defined signatures based on population studies (Sanjuan-Pla et al. 2013), but we have not seen any subpopulations of cells in either young and old mice from either strain (**Figure S8A-D**).

The absence of discernible subpopulations in our study does not in any way preclude functional heterogeneity, but it suggests that this heterogeneity may for example be "stochastic" (Till et al. 1964; Abkowitz et al. 1995; Kirkland 2004; Roeder et al. 2005), or related to a very small number of key genes (rather than a broad state), or manifest only under specific signals, such as those the transplanted cells may encounter upon transplantation (Trentin 1971; Metcalf 1998; Moore and Lemischka 2006). Another possibility is that the cell fate choice is coupled inextricably to cell cycle states, in which we have observed clear changes with age.

Compositional and coordinated expression changes associated with HSC aging

Aging could, in principle, be associated with changes in the frequency of certain phenotypes or expression programs (clonal selection model) or may be driven by the concerted change of cell intrinsic states across the entire population of old HSCs (global population shift model). Our results show evidence for both compositional changes and coordinated, population-wide shifts in cell states demonstrating the power of single-cell analysis in distinguishing these models. Upon aging, we observed a conserved reduction specifically of LT-HSCs in G1 phase reflecting a change in proportion of that subpopulation of

cells. Previous studies reported an entire spectrum of cell cycle changes ranging from increased, decreased to unchanged proliferation in old LT-HSCs (Flach et al. 2014). In our hands, cell cycle analyses consistently showed a decreased number of G1 cells in two mouse strains (C57BL/6 and DBA/2) and by two independent approaches: as inferred from single-cell RNA-seq data (in duplicate experiments done weeks apart, and based on entire gene signature) and by Ki67/Hoechst staining paired with BrdU. Interestingly, a recent study reported decreased expression of genes related to cell cycle, DNA replication, and DNA base excision repair (which are normally upregulated during G1/S) in old LT-HSCs (Sun et al. 2014). Our results suggest that this observation may not be due to downregulation of those genes across most old LT-HSCs, but rather due to a decreased proportion of the subset of G1/S cells that highly express those genes. Moreover, our single cell RNA-seq approach revealed an entire cell cycle trajectory based on co-expression of large number of genes that is consistent between cell types and species (**Figure S2**). Amidst quiescent cells, we detected expression programs that are observed in practically every single cell we sampled from each cell type, age and strain without identifiable discrete cell subsets within LT- and ST-HSCs.

Self-renewal *vs*. differentiation-biased expression programs in HSCs

Our analysis revealed an expression program of old HSCs that differs from young HSCs and is diametrically opposed to the expression program associated with differentiation (**Figure 3**). In particular, old ST-HSCs resembled transcriptionally young LT-HSCs, which may be related to the recent demonstration that adult ST-HSCs nearly fully self-renew and serve as the main source of hematopoietic maintenance in mice (Busch et al. 2015). This raises the possibility that HSCs can occupy distinct positions in gene expression space such that those that are closer to the state of differentiated cells have a higher propensity for differentiation (differentiation-biased), while those that are located in the opposite direction have a higher propensity for self-renewal (self-renewal-biased). Accordingly, aging could shift LT-HSCs towards the self-renewal-biased state and away from the differentiation-biased state (**Figure 7**).

This is consistent with a recently suggested link between aging and self-renewal (Sun et al. 2014). Taken together, age-associated accumulation of LT-HSCs and their functional decline may be a consequence of the imbalance between self-renewal and differentiation, in favor of the former, and this imbalance may be reflected by a self-renewal-biased expression program. While these changes have consequences for the early steps of hematopoiesis, it remains to be determined what effects these may cause to the entire hematopoiesis (e.g. clonal hematopoiesis (Holstege et al. 2014)). Additional studies would be required to test this hypothesis and examine the functional implications of a decrease in the differentiation-related expression signature and whether it reflects increased self-renewal capacity. This may require developments of new tools given that ST-HSCs are the main contributors to steady-state hematopoietic production in unperturbed conditions, while they are relatively short-lived in standard transplantation experiments (Busch et al. 2015).

Our analysis identified a set of genes whose expression is both aging and differentiation dependent (**Table S3**), and these include several potentially causal regulators of HSC self-renewal and differentiation. *Flt3* and *Cd34* have been implicated in HSC differentiation (Osawa et al. 1996; Adolfsson et al. 2001; Yang et al. 2005; Buza-Vidas et al. 2011) and are expressed at lower levels in old *vs*. young LT-HSCs. Notably, Flt3 is a cytokine tyrosine kinase receptor, which is mutated in about a third of acute myeloid leukemia patients (Small 2006). Conversely, *Nfia*, *Id2* and *Itgb3* have been implicated in self-renewal (Miller et al. 2013; Imayoshi and Kageyama 2014; van Galen et al. 2014) and are expressed at higher levels in old *vs*. young LT-HSC. Dedicated studies are required to characterize these putative candidates in this context.

A cell cycle-dependent interplay between aging and differentiation

We observed a depletion in cells in the late G1 phase in old LT-HSCs, suggesting a faster transition through G1 and into S, which may shed light on the reduced expression of cell cycle related genes that was previously observed in old HSCs at the population level (Chambers et al. 2007; Sun et al. 2014). This

is reminiscent of the short G1 phase in mouse and human embryonic stem cells. In ESCs this is achieved by avoiding a normal G1 checkpoint, which shifts the balance from differentiation to self-renewal (Savatier et al. 1994; White et al. 2005). Old LT-HSCs might avoid the G1 checkpoint through the same or distinct mechanisms. Interestingly, one of the genes whose expression increases with age and decreases with differentiation (thereby is maximally expressed in old LT-HSCs) was Polo-like kinase 2 (PLK2), a known checkpoint regulator that controls progression during G1 and early S phases [reviewed in (van de Weerdt and Medema 2006)]. PLK2 inactivation was shown to extend the length of the cell cycle and delayed the entry into S phase (Ma et al. 2003), suggesting that PLK2 upregulation in old LT-HSC could facilitate rapid progression through G1.

Since asymmetric distribution of cell-fate determinants enables two daughter cells to follow different fates, the cell cycle may be linked to cell fate through the establishment of cell polarity, as shown in *C. elegans* and *Drosophila melanogaster* (Noatynska et al. 2013). Previous work has shown that young LT-HSCs undergo both symmetric and asymmetric division, and that the precise balance between the two is affected by various signals (Wu et al. 2007). Furthermore, LT-HSCs become largely apolar with age (Florian et al. 2012), raising the possibility that the aging-related changes described here are linked to the loss of cell polarity. Accordingly, it is possible that apolar old LT-HSCs, which traverse through G1 phase faster than their younger counterparts, undergo preferential symmetric divisions, thereby leading to amassing of LT-HSCs with age.

Taken together, it is tempting to speculate that the accumulation of LT-HSCs, their short G1 phase and self-renewal-biased expression program are mechanistically coupled. This could be accomplished either by an altered cell cycle progression and a shorter G1 phase driving a self-renewal-biased expression program, or by an expression program affecting the cell cycle, which, in turn, results in a shorter G1 phase. Either scenario may ultimately lead (perhaps through loss of polarity) to a symmetric cell division, where both daughter cells maintain LT-HSC identity and, thereby, driving the increase of LT-HSCs

frequencies in bone marrow and at the same time to a disproportionally smaller number of differentiated cells (*i.e.* ST-HSCs in LSK compartment). Additional work will be required to further examine these possibilities and the role of potential candidate genes such as PLK2 in the connection between cell cycle, aging and differentiation-related expression states.

Methods

Isolation of hematopoietic stem and progenitor cells

Young (2-3 months old) female C57BL/6 and DBA/2 mice were purchased from Taconic and The Jackson Laboratory respectively. Old female C57BL/6 (>22 months old) and DBA/2 (20 months old) mice were obtained from the National Institute of Aging Mice and housed in the Boston Children's Hospital Animal facility (IACUC 1012-104-15).

For single cell sorting (BD FACS AriaII), total bone marrow (BM) cells were isolated from long bones, underwent erythrocyte lysis and CD117-enrichment prior to antibody staining (CD11b, Gr1, CD45R, CD3e, TER119, CD117, Sca1, CD48, CD150, all from eBioscience and Biolegend). LT-HSCs, ST-HSCs and MPPs were double-sorted into 96-well plates pre-loaded with 5µl of lysis buffer (TCL lysis buffer, Qiagen) supplemented with 1% (v/v) 2-mercaptoethanol (Qiagen) and flash frozen. For populations, cells were sorted directly into lysis buffer and RNA extracted using PrepEase (Affymetrix).

For cell cycle, we used BD Cytofix/Cytoperm and Ki-67 kit (BD) following the manufacturer's instructions.

For *in vivo* bromodeoxyuridine (BrdU) incorporation, mice were intraperitoneally injected with two doses of BrdU (BD Pharmingen), 8 and 2 hours before sacrifice, at 50 µg/g b.wt. and used BrdU Flow Kit (BD Pharmingen) for detection.

For colony-formation assays, 250 FACS-sorted LT-HSCs or ST-HSCs from young and old C57BL/6 mice were plated on MethoCult (M3434, Stem Cell Technologies) according to the manufacturer's instructions. The colonies were counted on day 10.

RNA-seq library preparation and initial data processing

We prepared and profiled libraries as previously described (Patel et al. 2014) from 1,152 individual cells. Sequencing data was processed as previously described (Patel et al. 2014). Before all subsequent

analyses, we filtered and centered the data. First, we filtered out cells with less than 2,500 genes with $\log_2(TPM+1) > 2$. Second, we excluded genes whose $\log_2(TPM+1) < 4$ in the aggregated data for each of the 6 populations. Third, we centered the data by subtracting for each gene its average expression ($\log_2(TPM+1)$) across all cells. Matlab's PCA function was used with default parameters.

Clustering based analysis of cell cycle state

Cell cycle genes were defined as those with a "cell cycle process" Gene Ontology annotation (downloaded from MSigDB version 3.1) (Reference Genome Group of the Gene Ontology 2009) or identified as cycling in HeLa cells (Whitfield et al. 2002). We defined four cell cycle signatures (G1/S, S, G2/M and M) as the average expression ($\log_2(TPM+1)$) of phase-specific subsets of the cell cycle genes as defined previously in synchronized HeLa cells (Whitfield et al. 2002). We refined these signatures by averaging only over those genes whose expression pattern in our data correlated highly ($r>0.5$) with the average signature of the respective cell cycle phase (before excluding any gene), in order to remove the influence of genes that were previously detected in HeLa cells but do not appear to cycle in our data.

High-resolution analysis of cell cycle progression

Plotting the average of the G1/S and S signatures *vs*. the average of the G2/M and M signatures for each cell (**Figure 2D** and **S3A**) showed an approximate circle, which we assume reflects all phases of the cell cycle. Based on this assumption we ordered all cells according to the apparent progression along the cell cycle and assigned a rank of cell cycle progression to each cell (**Figure S3A** and **Table S1**).

Identification of aging- and differentiation-dependent differentially expressed genes

Two-sample *t*-tests with a *p*-value of 0.05 and no correction for multiple testing were initially used to identify potentially significant differential expression in comparison of each pair of populations with matched cell types but different age (age effects) or matched age but different cell type (differentiation effects).

Data access

Sequencing data from this study have been submitted to the NCBI Gene Expression Omnibus (GEO; http://www.ncbi.nlm.nih.gov/geo/) under accession number GSE59114.

Supplementary Material

There are supplementary methods and 8 figures associated with this manuscript.

Acknowledgements

We thank Alex Shalek, Rahul Satija, Orit Rozenblatt-Rosen and Dawn Thompson for scientific discussions, Candace Guiducci for project management, Leslie Gaffney for assistance with artwork, and the Broad Genomics Platform for all sequencing work. We thank DFCI and Joslin/HSCI Flow Cytometry Cores for excellent flow cytometry support.

This work was supported by an EHA Research Fellowship award from the European Hematology Association (MSK), EMBO Long Term Fellowship (MSK), HFSP Long Term Fellowship (IT), Rothschild Fellowship (IT), German Cancer Foundation (DH), Leukemia and Lymphoma Society Scholar Award (BLE), NIH (P01 CA066996) (BLE), HHMI (AR), NIH CEGS Award (1P50HG006193-01, AR), and the Klarman Family Foundation (AR). A.J.W. is an Early Career Scientist of the Howard Hughes Medical Institute.

Figure Legends

Figure 1. Single-cell RNA-seq of young and old HSCs

(**A**) Overview of experimental design. (**B, C**) Sorting strategy for isolating LT-HSCs (LSK $CD48^-$ $CD150^+$), ST-HSCs (LSK $CD48^-CD150^-$) and MPPs (LSK $CD48^+CD150^-$) from young (**B**) and old (**C**) C57BL/6 mice. (**D, E**) LT-HSC compartment expands during aging. Shown are frequencies of LT-HSC, ST-HSC, and MPPs (*x*-axis) in young (black) and old (white) C57BL/6 mice as percentage of bone marrow (**D**) or stem cell compartment (lineage$^-$ $SCA1^+KIT^+$, LSK, **E**). Statistically significant differences are indicated by *** ($p<0.001$), ** ($p<0.01$), * ($p<0.05$), n=8-10. (**F**) Single cell RNA-seq recapitulates population RNA-seq. Shown are expression levels for all genes calculated from RNA-seq of a population of young LT-HSCs (*x* axis) and by averaging expression levels from ~200 single young LT-HSCs (*y* axis). The Pearson correlation coefficient (r=0.9) is denoted. Grey scale bar: gene density. (**G**) Heat map of Pearson correlation coefficients (*r*, color bar) between pairs of RNA-seq profiles of populations (columns) and matching averaged single-cell data (rows) from C57BL/6. (**H**) RNA-seq coverage of known cell surface markers in representative cells from young C57BL/6 mice [plot generated by the Integrative Genome Viewer 2.3 (Robinson et al. 2011; Thorvaldsdottir et al. 2013)].

Figure 2. Old LT-HSCs have a lower frequency of cells in G1 phase of the cell cycle

(**A**) The top eight PCs in each cell type and age. Shown is the percentage of annotated cell cycle genes (*y* axis) in the top 100 genes that correlate with each of the PCs (*x* axis) in each population. **(B)** Cell cycle analysis on mouse KIT enriched bone marrow cells stained with Pyronin Y (*y*-axis) and Hoechst (*x*-axis), reflecting for each cell the amount of RNA and DNA, respectively. Sorting gates and cell cycle phases are indicated. **(C)** RNA-seq of KIT enriched bone marrow cells at different cell cycle phases. Shown is the average expression of G1/S genes (*x* axis) and G2/M genes (*y* axis) from RNA sequenced from gates in (C) (color coded). **(D)** HSC single cell transcriptomes can be clustered by their cell cycle status. Heat map shows average expression of cell cycle phases gene signatures (rows) in each cell (column). The cells are partitioned into three clusters expressing the G1/S program, G2/M program or neither. **(E)** Cell cycle distribution changes as a function of cell type and age. Percentage of cells in cluster 1 (G2/M, grey) and cluster 2 (G1/S, black), within each cell type, for young (*x*-axis) and old (*y*-axis) HSCs. (**F**) Cell cycle trajectory inferred from single cell RNA-seq. Shown is the average expression of G1/S genes (*x* axis) and G2/M genes (*y* axis). The arrow and labels reflect inferred cell cycle progression. **(G, H)** Lower frequency of G1 cells among old LT-HSCs based on FACS analysis. (**G**) Shown are cell frequencies in G1 (black) and S-G2-M (grey) in cells from young (*x*-axis) and old (*y*-axis) mice based on intracellular staining with Ki67/Hoechst. (**H**) Representative FACS plots for young and old LT-HSCs from C57BL/6 mice. (**I**) The frequency of young and old LT-HSCs in S phase based on *in vivo* BrdU incorporation. (**J**) Representative BrdU FACS plots for young and old LT-HSCs from C57BL/6 mice.

Figure 3. HSC aging and differentiation are associated with opposite expression programs

A joint PCA was performed for all non-cycling cells, and each of the top 2 PCs distinguishes cells by their cell type and age, with higher scores for young and differentiated HSCs and lower scores for old and less-differentiated cells. (**A-D**) Each plot shows the loadings of PC1 and PC2, colored based on their cell type and age for cells from all six populations (A) or from specific pairs of populations that differ by age (B), differentiation (C), or both (D). (**E**) Distribution of PC1+PC2 scores for young (top) and old (bottom) LT- and ST- HSCs. Aging is associated with a decrease in, and differentiation is associated with an increase in, the PC1+PC2 scores. (**F**) Colony formation assays using methylcellulose. 250 of either young or old LT- and ST-HSCs were plated on methylcellulose (n=5). Colonies were counted on day 10. The colony numbers are averages of duplicate measurements of each individual mouse. Statistically significant differences are indicated by *** ($p<0.001$), ** ($p<0.01$), * ($p<0.05$). (**G**) Distribution of the megakaryocyte progenitor (MkP) signature scores, defined as the average normalized expression of MkP-enriched genes (Sanjuan-Pla et al. 2013) (*x*-axis) for LT-HSC (red), ST-HSC (blue) and MPP (green) in young (top panel) and old (bottom panel) mice.

Figure 4. An inverse relationship between the transcriptional signatures of aging and differentiation

(A) A gene signature of aging and differentiation. Left: Heatmap showing the relative expression levels of 77 genes (rows) significantly associated with aging and differentiation, in all non-cycling cells of LT- and ST- HSCs. Cells (columns) are sorted by age and within each age by cell type. Genes above horizontal black bar are higher in LT- than ST-HSCs and in old *vs*. young cells. Genes below the horizontal black bar are higher in ST- than LT-HSCs and in young *vs*. old cells. Right: the average expression of each gene (row) over all the non-cycling cells from each combination of cell type and age (column). **(B)** Genes in the signature have correlated loadings on PC1 and PC2. Shown are the PC1 (*x* axis) and PC2 (*y* axis) loadings for each gene. Genes in the signature in (B) are marked in large points, colored in blue and red, respectively for either high or low loadings for both PCs. **(C)** CD34 and FLT3 protein are both decreased with age and increased with differentiation. Shown are the median fluorescence intensity (MFI, *y*-axis) of fluorescent-conjugated FLT3 (left) and CD34 (right) protein in young and old LT-HSC (black) and ST-HSCs (grey).

Figure 5. Subsets of cells with lymphoid and myeloid-like transcriptional bias are discernible within immunophenotypically defined MPPs in C57BL/6 mice

(**A-C**) MPPs profiles are not distinguishable by age. PCA was performed independently for non-cycling cells of each of LT-HSCs (**A**), ST-HSCs (**B**) and MPPs (**C**). Each plot shows the loadings of PC1 and PC2, colored based on cell type and age. Higher scores for young HSCs and lower scores for old cells are characteristic for LT-HSCs (**A**) and ST-HSCs (**B**), but not for MPPs (**C**). (**D**) Two distinct modules in MPPs. Heat map shows the expression of genes from two distinct gene sets (rows; gene set 1 – lymphoid-biased; and gene set 2 – myeloid-biased) across all non-cycling MPPs (columns). (**E**) Non-cycling MPPs from both young and old mice form a continuous spectrum along the two states. Shown are the signature scores (average normalized expression of gene set1 minus that of gene-set2) for each non-cycling MPP from young (dark green) or old (light green) mouse. MPPs are ranked by increasing scores (*x*-axis). (**F**) Gene set enrichment analysis based on defined progenitor sets (CLP, MkP and preMegE) within gene sets (gene set 1 and gene set 2) defining two subsets of MPPs in C57BL/6.

Figure 6. Age associated changes are conserved in DBA/2

(**A**) Gating strategy used to isolate LT-HSCs (LSK $CD150^{+}CD48^{-}$), ST-HSCs (LSC $CD150^{-}CD48^{-}$) and MPPs (LSK $CD150^{-}CD48^{+}$) from the bone marrow of young (6–12 weeks) DBA/2 mice. (**B**) LT-HSC compartment expands during aging. Shown are frequencies of LT-HSC, ST-HSC, and MPPs (*x*-axis) in young (black) and old (white) DBA/2 mice as percentage of bone marrow. Statistically significant differences are indicated by *** ($p<0.001$). **(C)** Cell cycle trajectory inferred from single cell RNA-seq. Shown is the average expression of G1/S genes (*x*-axis) and G2/M genes (*y*-axis). The arrow and labels reflect inferred cell cycle progression. (**D**) Representative FACS plots for Ki67/Hoechst intracellular staining in young and old LT-HSCs from DBA/2 mice. (**E**) Cell cycle distribution changes with age. Top: Cells were ordered according to their inferred cell cycle progression and the average expression of G1/S, S, and G2/M genes (*y* axis, curves from dark to light grey) was calculated with a sliding window of 11 cells (*x* axis). The first ~217 cells are 'non cycling' and only a small portion of them is depicted in the graph. The G0/G1 approximate border was defined as the first position with a positive G1/S score (*i.e.* above the average of all cells) and other borders were approximated by manual inspection of the figure. Bottom: For each cell type, shown is the $\log_2$ of the ratio between percentages of old cells divided by the percentage of young cells along the inferred cell cycle progression (with a sliding window of 100 cells). Shaded colors reflect the inferred cell cycle phases; cells are ordered by the analysis of the top panel. (**F**) Distribution of the C57BL/6 derived signature scores for young and old LT- and ST-HSCs, defined as the average normalized expression of young LT-HSC (dark red), old LT-HSC (light red), young ST-HSC (dark blue) and old ST-HSC (light blue) enriched genes (*x*-axis) respectively.

Figure 7. A model of age-dependent changes in LT-HSCs

Young LT-HSCs (red, top) maintain an appropriate balance between efficient self-renewal (semi-circular arrow) and differentiation into ST-HSCs (horizontal arrow) that then further differentiate to reconstitute hematopoiesis. In contrast, old LT-HSCs (bottom) are inappropriately shifted towards self-renewal (thick semi-circular arrow) and thereby an accumulation of LT-HSCs (depicted by more copies of old LT-HSCs), ST-HSCs reduction (depicted by less copies of ST-HSCs) and less efficient reconstitution of hematopoiesis (dashed arrow). This can be due to either a short G1, which limits the capacity of old LT-HSCs to receive differentiation signals, or to an expression program that resembles a less differentiated state and might reflect defects in differentiation, or to both, as these might be causally linked.

References

Abkowitz JL, Persik MT, Shelton GH, Ott RL, Kiklevich JV, Catlin SN, Guttorp P. 1995. Behavior of hematopoietic stem cells in a large animal. *Proceedings of the National Academy of Sciences of the United States of America* **92**: 2031-2035.

Adolfsson J, Borge OJ, Bryder D, Theilgaard-Monch K, Astrand-Grundstrom I, Sitnicka E, Sasaki Y, Jacobsen SE. 2001. Upregulation of Flt3 expression within the bone marrow Lin(-)Sca1(+)c-kit(+) stem cell compartment is accompanied by loss of self-renewal capacity. *Immunity* **15**: 659-669.

Beerman I, Bhattacharya D, Zandi S, Sigvardsson M, Weissman IL, Bryder D, Rossi DJ. 2010. Functionally distinct hematopoietic stem cells modulate hematopoietic lineage potential during aging by a mechanism of clonal expansion. *Proceedings of the National Academy of Sciences of the United States of America* **107**: 5465-5470.

Beghe C, Wilson A, Ershler WB. 2004. Prevalence and outcomes of anemia in geriatrics: a systematic review of the literature. *The American journal of medicine* **116 Suppl 7A**: 3S-10S.

Benveniste P, Frelin C, Janmohamed S, Barbara M, Herrington R, Hyam D, Iscove NN. 2010. Intermediate-term hematopoietic stem cells with extended but time-limited reconstitution potential. *Cell stem cell* **6**: 48-58.

Busch K, Klapproth K, Barile M, Flossdorf M, Holland-Letz T, Schlenner SM, Reth M, Höfer T, Rodewald H-R. 2015. Fundamental properties of unperturbed haematopoiesis from stem cells in vivo. *Nature* doi:10.1038/nature14242.

Buza-Vidas N, Woll P, Hultquist A, Duarte S, Lutteropp M, Bouriez-Jones T, Ferry H, Luc S, Jacobsen SE. 2011. FLT3 expression initiates in fully multipotent mouse hematopoietic progenitor cells. *Blood* **118**: 1544-1548.

Calegari F, Huttner WB. 2003. An inhibition of cyclin-dependent kinases that lengthens, but does not arrest, neuroepithelial cell cycle induces premature neurogenesis. *Journal of cell science* **116**: 4947-4955.

Challen GA, Boles NC, Chambers SM, Goodell MA. 2010. Distinct hematopoietic stem cell subtypes are differentially regulated by TGF-beta1. *Cell stem cell* **6**: 265-278.

Chambers SM, Shaw CA, Gatza C, Fisk CJ, Donehower LA, Goodell MA. 2007. Aging hematopoietic stem cells decline in function and exhibit epigenetic dysregulation. *PLoS biology* **5**: e201.

Coronado D, Godet M, Bourillot PY, Tapponnier Y, Bernat A, Petit M, Afanassieff M, Markossian S, Malashicheva A, Iacone R et al. 2013. A short G1 phase is an intrinsic determinant of naive embryonic stem cell pluripotency. *Stem cell research* **10**: 118-131.

de Haan G, Nijhof W, Van Zant G. 1997. Mouse strain-dependent changes in frequency and proliferation of hematopoietic stem cells during aging: correlation between lifespan and cycling activity. *Blood* **89**: 1543-1550.

Dykstra B, Kent D, Bowie M, McCaffrey L, Hamilton M, Lyons K, Lee SJ, Brinkman R, Eaves C. 2007. Long-term propagation of distinct hematopoietic differentiation programs in vivo. *Cell stem cell* **1**: 218-229.

Dykstra B, Olthof S, Schreuder J, Ritsema M, de Haan G. 2011. Clonal analysis reveals multiple functional defects of aged murine hematopoietic stem cells. *The Journal of experimental medicine* **208**: 2691-2703.

Flach J, Bakker ST, Mohrin M, Conroy PC, Pietras EM, Reynaud D, Alvarez S, Diolaiti ME, Ugarte F, Forsberg EC et al. 2014. Replication stress is a potent driver of functional decline in ageing haematopoietic stem cells. *Nature* **512**: 198-202.

Florian MC, Dorr K, Niebel A, Daria D, Schrezenmeier H, Rojewski M, Filippi MD, Hasenberg A, Gunzer M, Scharffetter-Kochanek K et al. 2012. Cdc42 activity regulates hematopoietic stem cell aging and rejuvenation. *Cell stem cell* **10**: 520-530.

Fox RR, ed. 1997. *Handbook on Genetically Standardized JAX Mice*, Jackson Laboratory, Bar Harbor, ME.

Guo S, Zi X, Schulz VP, Cheng J, Zhong M, Koochaki SH, Megyola CM, Pan X, Heydari K, Weissman SM et al. 2014. Nonstochastic reprogramming from a privileged somatic cell state. *Cell* **156**: 649-662.

Hashimshony T, Wagner F, Sher N, Yanai I. 2012. CEL-Seq: single-cell RNA-Seq by multiplexed linear amplification. *Cell reports* **2**: 666-673.

Holstege H, Pfeiffer W, Sie D, Hulsman M, Nicholas TJ, Lee CC, Ross T, Lin J, Miller MA, Ylstra B et al. 2014. Somatic mutations found in the healthy blood compartment of a 115-yr-old woman demonstrate oligoclonal hematopoiesis. *Genome Res* **24**: 733-742.

Imayoshi I, Kageyama R. 2014. bHLH factors in self-renewal, multipotency, and fate choice of neural progenitor cells. *Neuron* **82**: 9-23.

Jojic V, Shay T, Sylvia K, Zuk O, Sun X, Kang J, Regev A, Koller D, Best AJ, Knell J et al. 2013. Identification of transcriptional regulators in the mouse immune system. *Nature immunology* **14**: 633-643.

Kafri R, Levy J, Ginzberg MB, Oh S, Lahav G, Kirschner MW. 2013. Dynamics extracted from fixed cells reveal feedback linking cell growth to cell cycle. *Nature* **494**: 480-483.

Kent DG, Copley MR, Benz C, Wohrer S, Dykstra BJ, Ma E, Cheyne J, Zhao Y, Bowie MB, Zhao Y et al. 2009. Prospective isolation and molecular characterization of hematopoietic stem cells with durable self-renewal potential. *Blood* **113**: 6342-6350.

Kiel MJ, Yilmaz OH, Iwashita T, Yilmaz OH, Terhorst C, Morrison SJ. 2005. SLAM family receptors distinguish hematopoietic stem and progenitor cells and reveal endothelial niches for stem cells. *Cell* **121**: 1109-1121.

Kim M, Moon HB, Spangrude GJ. 2003. Major age-related changes of mouse hematopoietic stem/progenitor cells. *Annals of the New York Academy of Sciences* **996**: 195-208.

Kirkland MA. 2004. A phase space model of hemopoiesis and the concept of stem cell renewal. *Experimental hematology* **32**: 511-519.

Li VC, Ballabeni A, Kirschner MW. 2012. Gap 1 phase length and mouse embryonic stem cell self-renewal. *Proceedings of the National Academy of Sciences of the United States of America* **109**: 12550-12555.

Liang Y, Van Zant G, Szilvassy SJ. 2005. Effects of aging on the homing and engraftment of murine hematopoietic stem and progenitor cells. *Blood* **106**: 1479-1487.

Lichtman MA, Rowe JM. 2004. The relationship of patient age to the pathobiology of the clonal myeloid diseases. *Seminars in oncology* **31**: 185-197.

Linton PJ, Dorshkind K. 2004. Age-related changes in lymphocyte development and function. *Nature immunology* **5**: 133-139.

Ma S, Charron J, Erikson RL. 2003. Role of Plk2 (Snk) in mouse development and cell proliferation. *Molecular and cellular biology* **23**: 6936-6943.

Macosko EZ, Basu A, Satija R, Nemesh J, Shekhar K, Goldman M, Tirosh I, Bialas AR, Kamitaki N, Martersteck EM et al. 2015. Highly Parallel Genome-wide Expression Profiling of Individual Cells Using Nanoliter Droplets. *Cell* **161**: 1202-1214.

Mahata B, Zhang X, Kolodziejczyk AA, Proserpio V, Haim-Vilmovsky L, Taylor AE, Hebenstreit D, Dingler FA, Moignard V, Gottgens B et al. 2014. Single-cell RNA sequencing reveals T helper cells synthesizing steroids de novo to contribute to immune homeostasis. *Cell reports* **7**: 1130-1142.

Massague J. 2004. G1 cell-cycle control and cancer. *Nature* **432**: 298-306.

Metcalf D. 1998. Lineage commitment and maturation in hematopoietic cells: the case for extrinsic regulation. *Blood* **92**: 345-347; discussion 352.

Miller PG, Al-Shahrour F, Hartwell KA, Chu LP, Jaras M, Puram RV, Puissant A, Callahan KP, Ashton J, McConkey ME et al. 2013. In Vivo RNAi screening identifies a leukemia-specific dependence on integrin beta 3 signaling. *Cancer cell* **24**: 45-58.

Moore KA, Lemischka IR. 2006. Stem cells and their niches. *Science* **311**: 1880-1885.

Morita Y, Ema H, Nakauchi H. 2010. Heterogeneity and hierarchy within the most primitive hematopoietic stem cell compartment. *The Journal of experimental medicine* **207**: 1173-1182.

Morrison SJ, Wandycz AM, Akashi K, Globerson A, Weissman IL. 1996. The aging of hematopoietic stem cells. *Nature medicine* **2**: 1011-1016.

Muller-Sieburg CE, Cho RH, Thoman M, Adkins B, Sieburg HB. 2002. Deterministic regulation of hematopoietic stem cell self-renewal and differentiation. *Blood* **100**: 1302-1309.

Muller-Sieburg CE, Sieburg HB, Bernitz JM, Cattarossi G. 2012. Stem cell heterogeneity: implications for aging and regenerative medicine. *Blood* **119**: 3900-3907.

Noatynska A, Tavernier N, Gotta M, Pintard L. 2013. Coordinating cell polarity and cell cycle progression: what can we learn from flies and worms? *Open biology* **3**: 130083.

Oguro H, Ding L, Morrison SJ. 2013. SLAM family markers resolve functionally distinct subpopulations of hematopoietic stem cells and multipotent progenitors. *Cell stem cell* **13**: 102-116.

Osawa M, Hanada K, Hamada H, Nakauchi H. 1996. Long-term lymphohematopoietic reconstitution by a single CD34-low/negative hematopoietic stem cell. *Science* **273**: 242-245.

Patel AP, Tirosh I, Trombetta JJ, Shalek AK, Gillespie SM, Wakimoto H, Cahill DP, Nahed BV, Curry WT, Martuza RL et al. 2014. Single-cell RNA-seq highlights intratumoral heterogeneity in primary glioblastoma. *Science* **344**: 1396-1401.

Pauklin S, Vallier L. 2013. The cell-cycle state of stem cells determines cell fate propensity. *Cell* **155**: 135-147.

Pronk CJ, Rossi DJ, Mansson R, Attema JL, Norddahl GL, Chan CK, Sigvardsson M, Weissman IL, Bryder D. 2007. Elucidation of the phenotypic, functional, and molecular topography of a myeloerythroid progenitor cell hierarchy. *Cell stem cell* **1**: 428-442.

Ramskold D, Luo S, Wang YC, Li R, Deng Q, Faridani OR, Daniels GA, Khrebtukova I, Loring JF, Laurent LC et al. 2012. Full-length mRNA-Seq from single-cell levels of RNA and individual circulating tumor cells. *Nature biotechnology* **30**: 777-782.

Reference Genome Group of the Gene Ontology C. 2009. The Gene Ontology's Reference Genome Project: a unified framework for functional annotation across species. *PLoS computational biology* **5**: e1000431.

Robinson JT, Thorvaldsdottir H, Winckler W, Guttman M, Lander ES, Getz G, Mesirov JP. 2011. Integrative genomics viewer. *Nature biotechnology* **29**: 24-26.

Roeder I, Kamminga LM, Braesel K, Dontje B, de Haan G, Loeffler M. 2005. Competitive clonal hematopoiesis in mouse chimeras explained by a stochastic model of stem cell organization. *Blood* **105**: 609-616.

Rossi DJ, Bryder D, Zahn JM, Ahlenius H, Sonu R, Wagers AJ, Weissman IL. 2005. Cell intrinsic alterations underlie hematopoietic stem cell aging. *Proceedings of the National Academy of Sciences of the United States of America* **102**: 9194-9199.

Sanjuan-Pla A, Macaulay IC, Jensen CT, Woll PS, Luis TC, Mead A, Moore S, Carella C, Matsuoka S, Jones TB et al. 2013. Platelet-biased stem cells reside at the apex of the haematopoietic stem-cell hierarchy. *Nature* **502**: 232-236.

Savatier P, Huang S, Szekely L, Wiman KG, Samarut J. 1994. Contrasting patterns of retinoblastoma protein expression in mouse embryonic stem cells and embryonic fibroblasts. *Oncogene* **9**: 809-818.

Shalek AK, Satija R, Adiconis X, Gertner RS, Gaublomme JT, Raychowdhury R, Schwartz S, Yosef N, Malboeuf C, Lu D et al. 2013. Single-cell transcriptomics reveals bimodality in expression and splicing in immune cells. *Nature* **498**: 236-240.

Shalek AK, Satija R, Shuga J, Trombetta JJ, Gennert D, Lu D, Chen P, Gertner RS, Gaublomme JT, Yosef N et al. 2014. Single-cell RNA-seq reveals dynamic paracrine control of cellular variation. *Nature* **509**: 363-369.

Shay T, Jojic V, Zuk O, Rothamel K, Puyraimond-Zemmour D, Feng T, Wakamatsu E, Benoist C, Koller D, Regev A. 2013. Conservation and divergence in the transcriptional programs of the human and

mouse immune systems. *Proceedings of the National Academy of Sciences of the United States of America* **110**: 2946-2951.

Sherr CJ. 2000. The Pezcoller lecture: cancer cell cycles revisited. *Cancer research* **60**: 3689-3695.

Small D. 2006. FLT3 mutations: biology and treatment. *Hematology / the Education Program of the American Society of Hematology American Society of Hematology Education Program* doi:10.1182/asheducation-2006.1.178: 178-184.

Sudo K, Ema H, Morita Y, Nakauchi H. 2000. Age-associated characteristics of murine hematopoietic stem cells. *The Journal of experimental medicine* **192**: 1273-1280.

Sun D, Luo M, Jeong M, Rodriguez B, Xia Z, Hannah R, Wang H, Le T, Faull KF, Chen R et al. 2014. Epigenomic profiling of young and aged HSCs reveals concerted changes during aging that reinforce self-renewal. *Cell stem cell* **14**: 673-688.

Takahashi T, Nowakowski RS, Caviness VS, Jr. 1995. The cell cycle of the pseudostratified ventricular epithelium of the embryonic murine cerebral wall. *The Journal of neuroscience : the official journal of the Society for Neuroscience* **15**: 6046-6057.

Thorvaldsdottir H, Robinson JT, Mesirov JP. 2013. Integrative Genomics Viewer (IGV): high-performance genomics data visualization and exploration. *Briefings in bioinformatics* **14**: 178-192.

Till JE, McCulloch EA, Siminovitch L. 1964. A Stochastic Model of Stem Cell Proliferation, Based on the Growth of Spleen Colony-Forming Cells. *Proceedings of the National Academy of Sciences of the United States of America* **51**: 29-36.

Trapnell C, Cacchiarelli D, Grimsby J, Pokharel P, Li S, Morse M, Lennon NJ, Livak KJ, Mikkelsen TS, Rinn JL. 2014. The dynamics and regulators of cell fate decisions are revealed by pseudotemporal ordering of single cells. *Nature biotechnology* **32**: 381-386.

Trentin JJ. 1971. Determination of bone marrow stem cell differentiation by stromal hemopoietic inductive microenvironments (HIM). *The American journal of pathology* **65**: 621-628.

Turturro A, Witt WW, Lewis S, Hass BS, Lipman RD, Hart RW. 1999. Growth curves and survival characteristics of the animals used in the Biomarkers of Aging Program. *The journals of gerontology Series A, Biological sciences and medical sciences* **54**: B492-501.

van de Weerdt BC, Medema RH. 2006. Polo-like kinases: a team in control of the division. *Cell cycle* **5**: 853-864.

van Galen P, Kreso A, Wienholds E, Laurenti E, Eppert K, Lechman ER, Mbong N, Hermans K, Dobson S, April C et al. 2014. Reduced lymphoid lineage priming promotes human hematopoietic stem cell expansion. *Cell stem cell* **14**: 94-106.

White J, Stead E, Faast R, Conn S, Cartwright P, Dalton S. 2005. Developmental activation of the Rb-E2F pathway and establishment of cell cycle-regulated cyclin-dependent kinase activity during embryonic stem cell differentiation. *Molecular biology of the cell* **16**: 2018-2027.

Whitfield ML, Sherlock G, Saldanha AJ, Murray JI, Ball CA, Alexander KE, Matese JC, Perou CM, Hurt MM, Brown PO et al. 2002. Identification of genes periodically expressed in the human cell cycle and their expression in tumors. *Molecular biology of the cell* **13**: 1977-2000.

Wills QF, Livak KJ, Tipping AJ, Enver T, Goldson AJ, Sexton DW, Holmes C. 2013. Single-cell gene expression analysis reveals genetic associations masked in whole-tissue experiments. *Nature biotechnology* **31**: 748-752.

Wilson A, Laurenti E, Oser G, van der Wath RC, Blanco-Bose W, Jaworski M, Offner S, Dunant CF, Eshkind L, Bockamp E et al. 2008. Hematopoietic stem cells reversibly switch from dormancy to self-renewal during homeostasis and repair. *Cell* **135**: 1118-1129.

Wu M, Kwon HY, Rattis F, Blum J, Zhao C, Ashkenazi R, Jackson TL, Gaiano N, Oliver T, Reya T. 2007. Imaging hematopoietic precursor division in real time. *Cell stem cell* **1**: 541-554.

Yang L, Bryder D, Adolfsson J, Nygren J, Mansson R, Sigvardsson M, Jacobsen SE. 2005. Identification of Lin(-)Sca1(+)kit(+)CD34(+)Flt3- short-term hematopoietic stem cells capable of rapidly reconstituting and rescuing myeloablated transplant recipients. *Blood* **105**: 2717-2723.

Yilmaz OH, Kiel MJ, Morrison SJ. 2006. SLAM family markers are conserved among hematopoietic stem cells from old and reconstituted mice and markedly increase their purity. *Blood* **107**: 924-930.

Figure 1

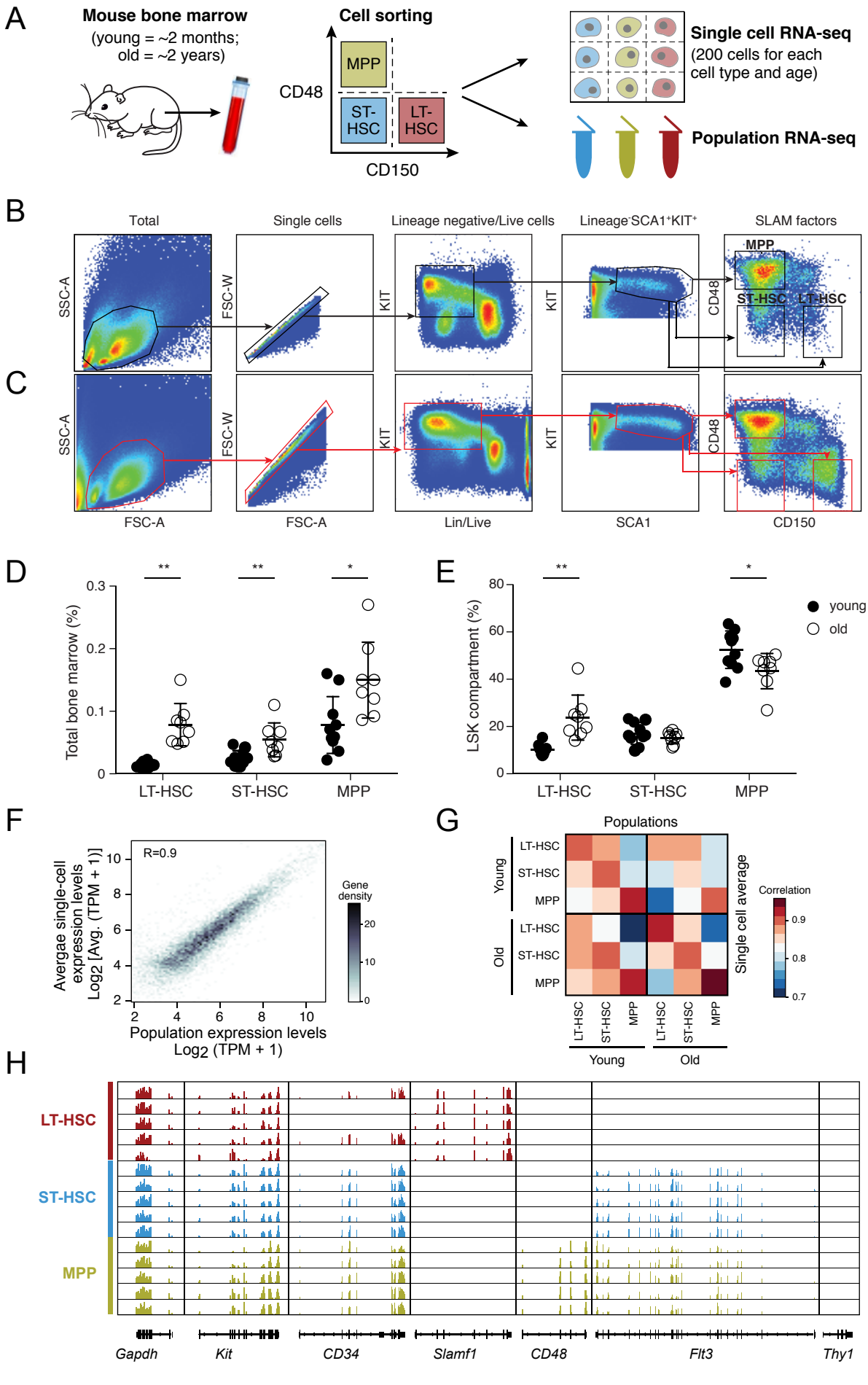

Figure 2

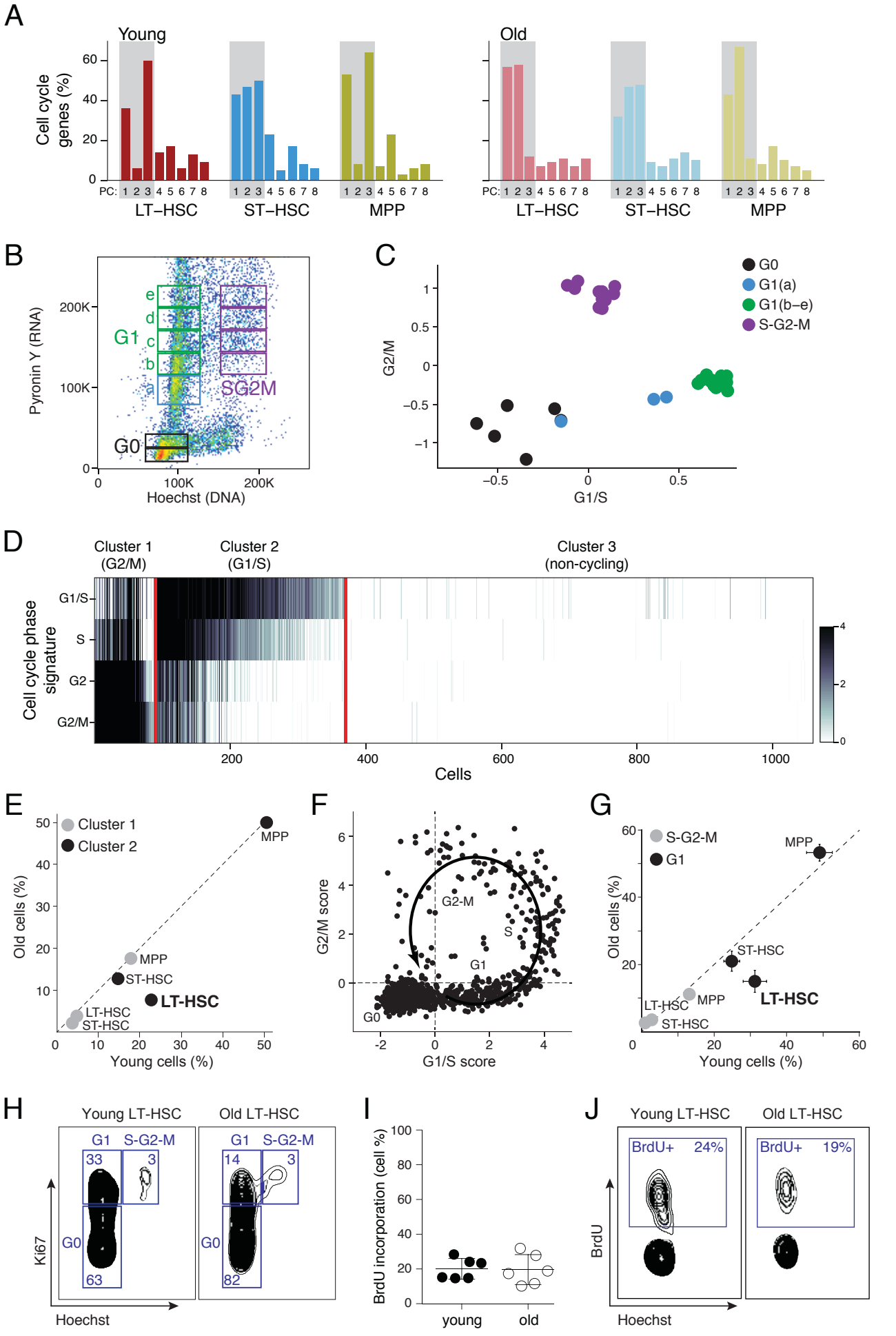

Figure 3

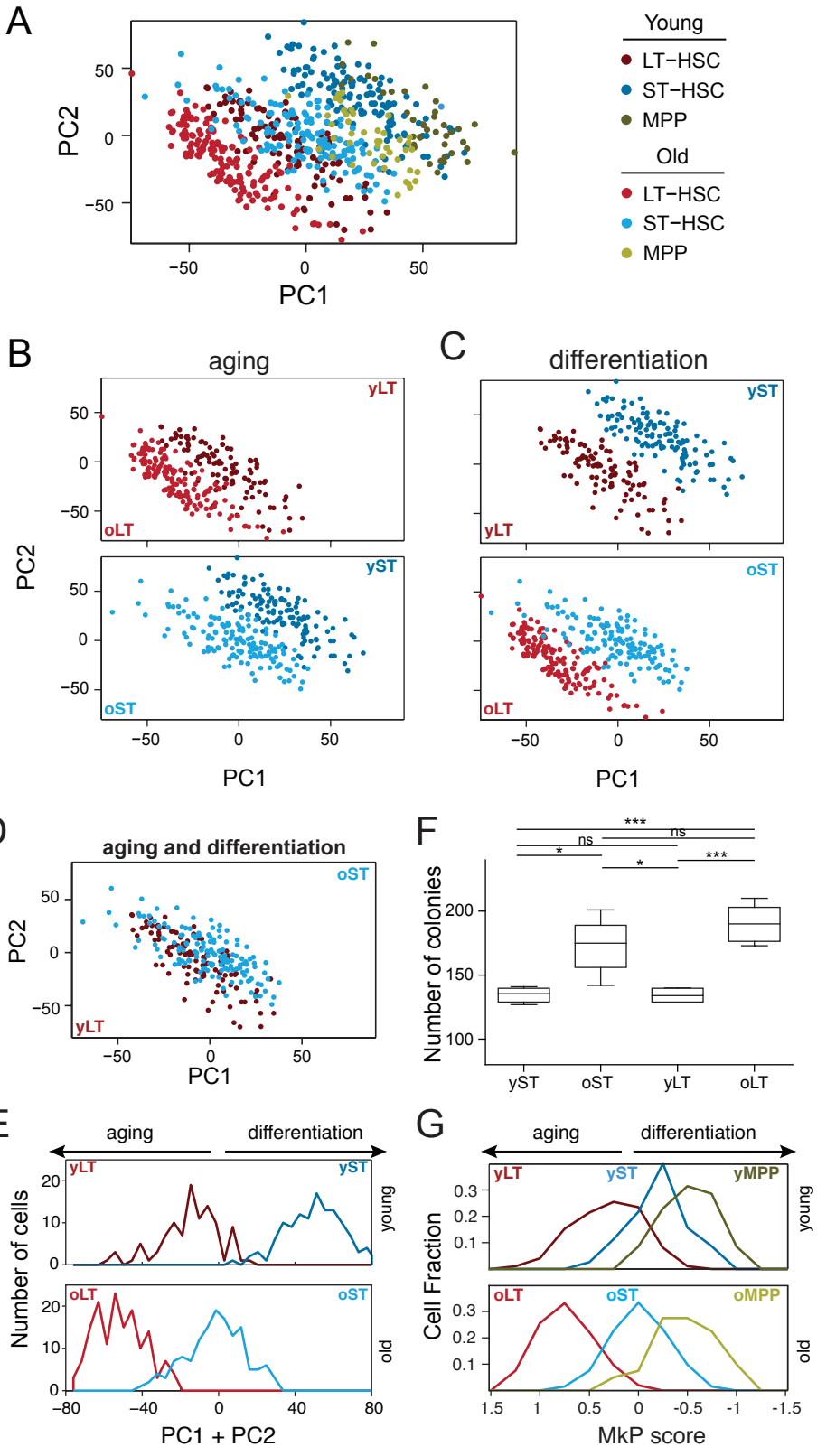

Figure 4

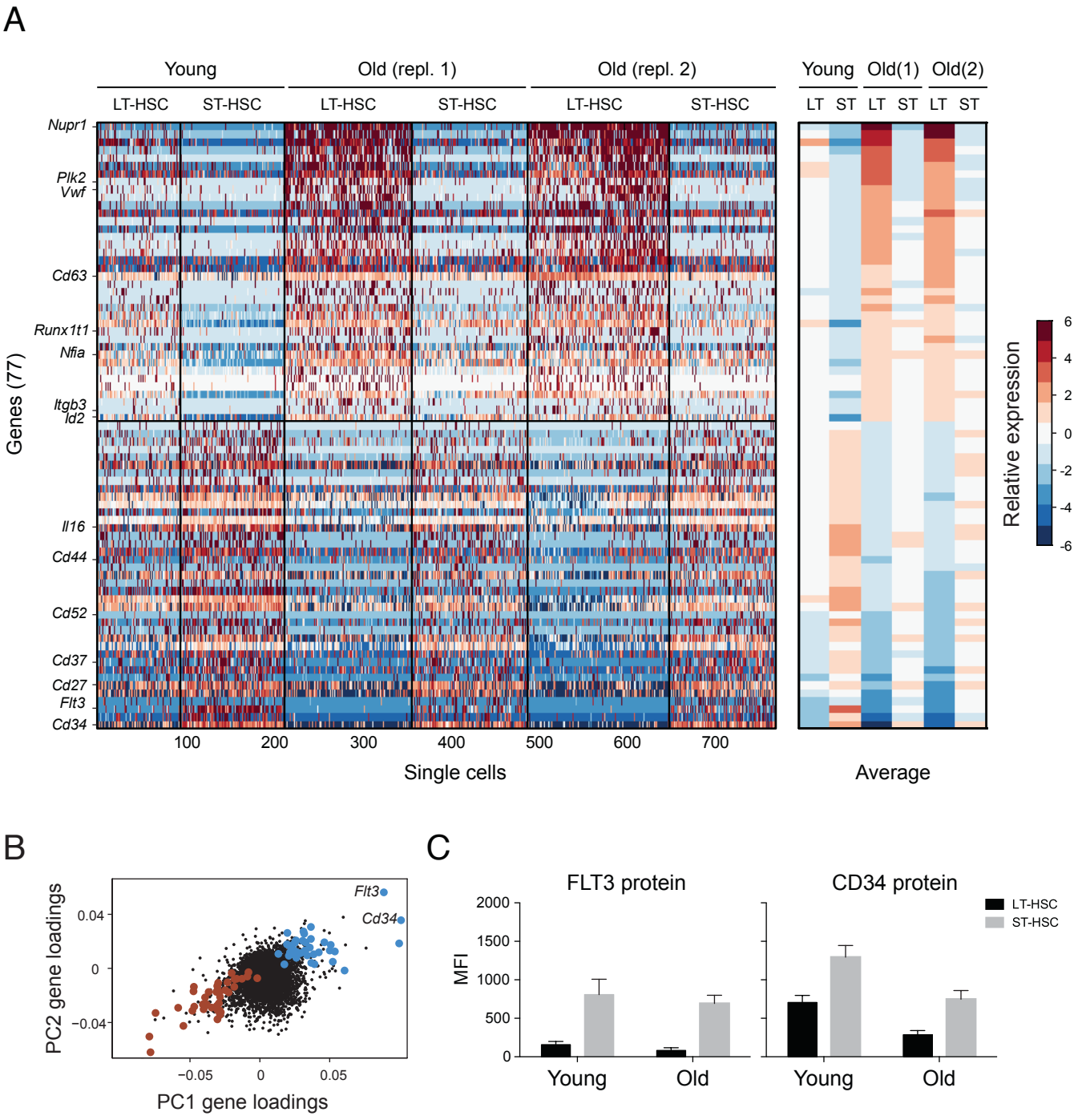

Figure 5

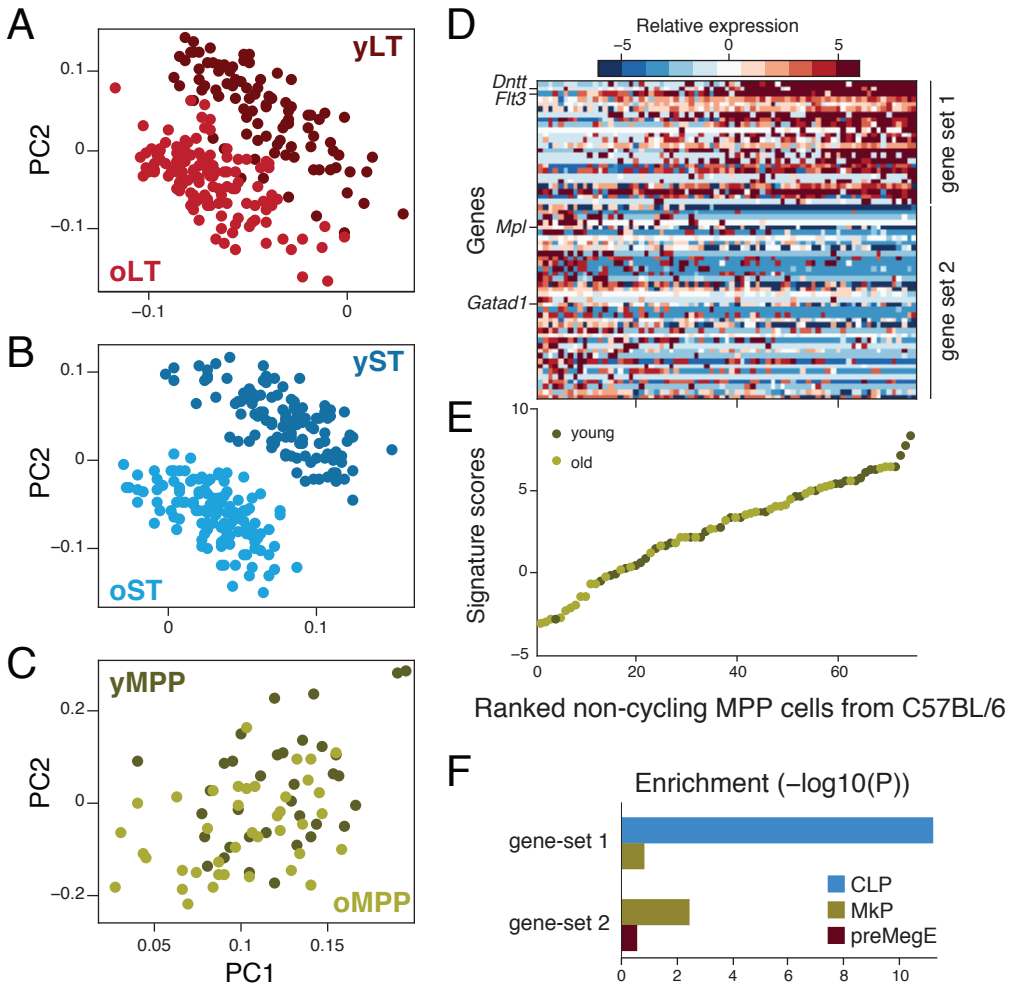

Figure 6

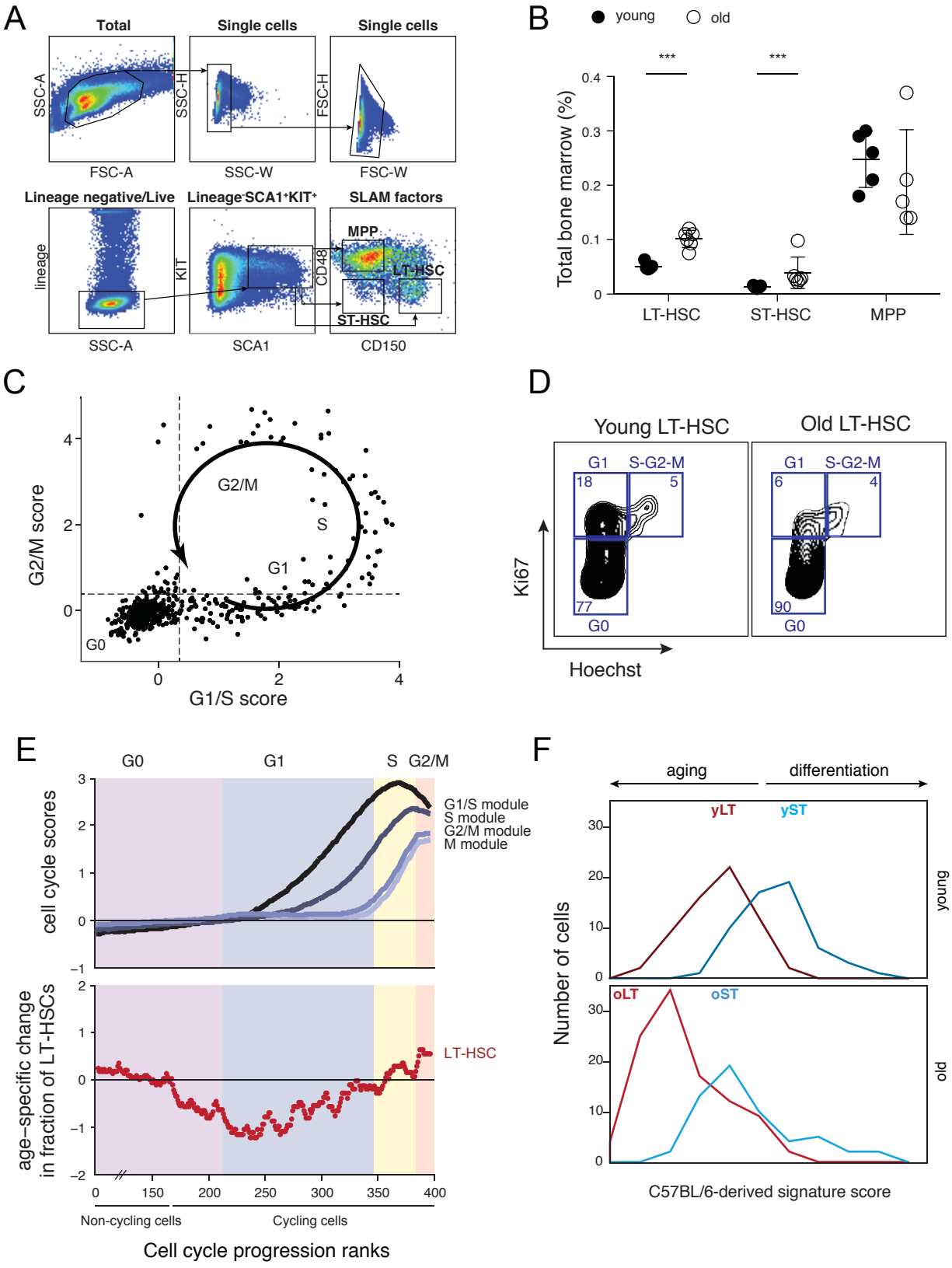

Figure 7

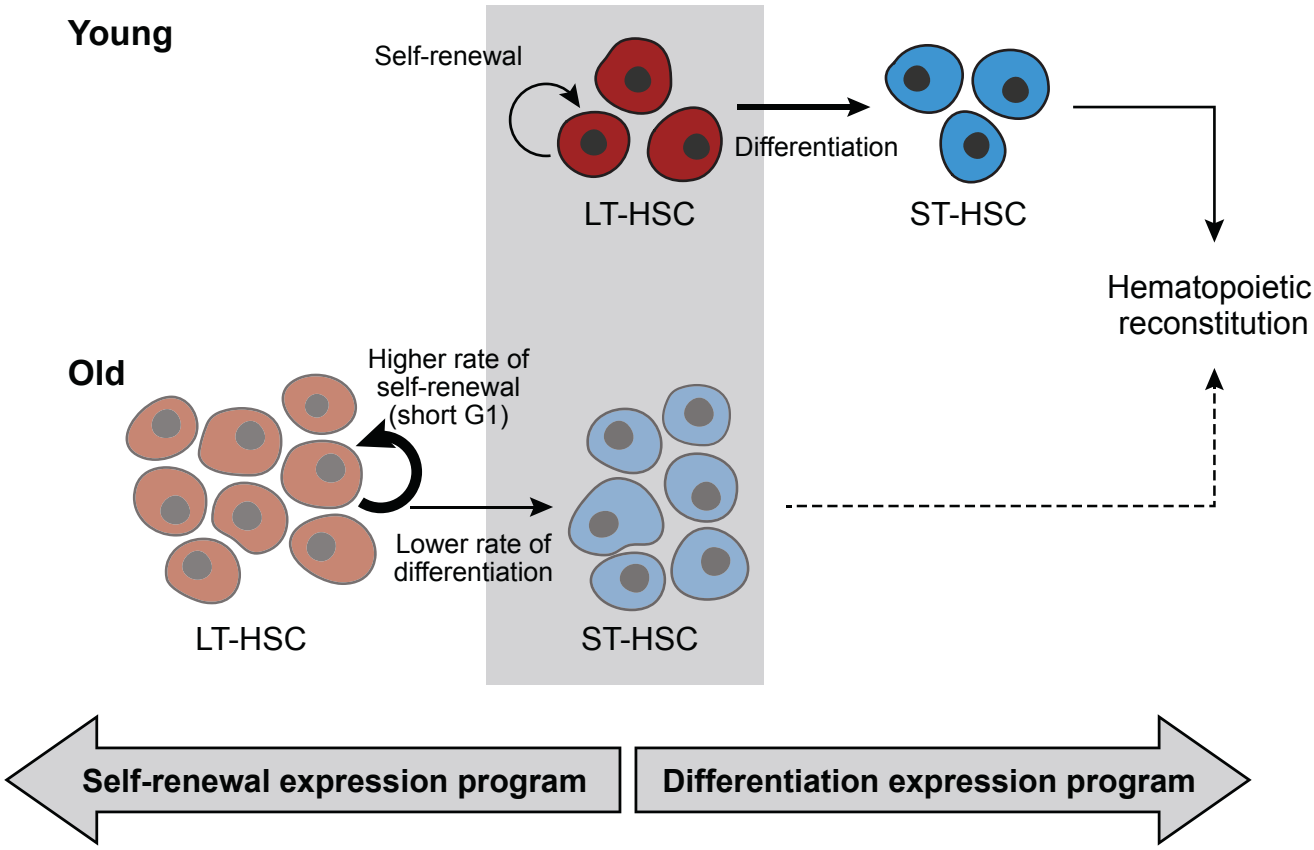

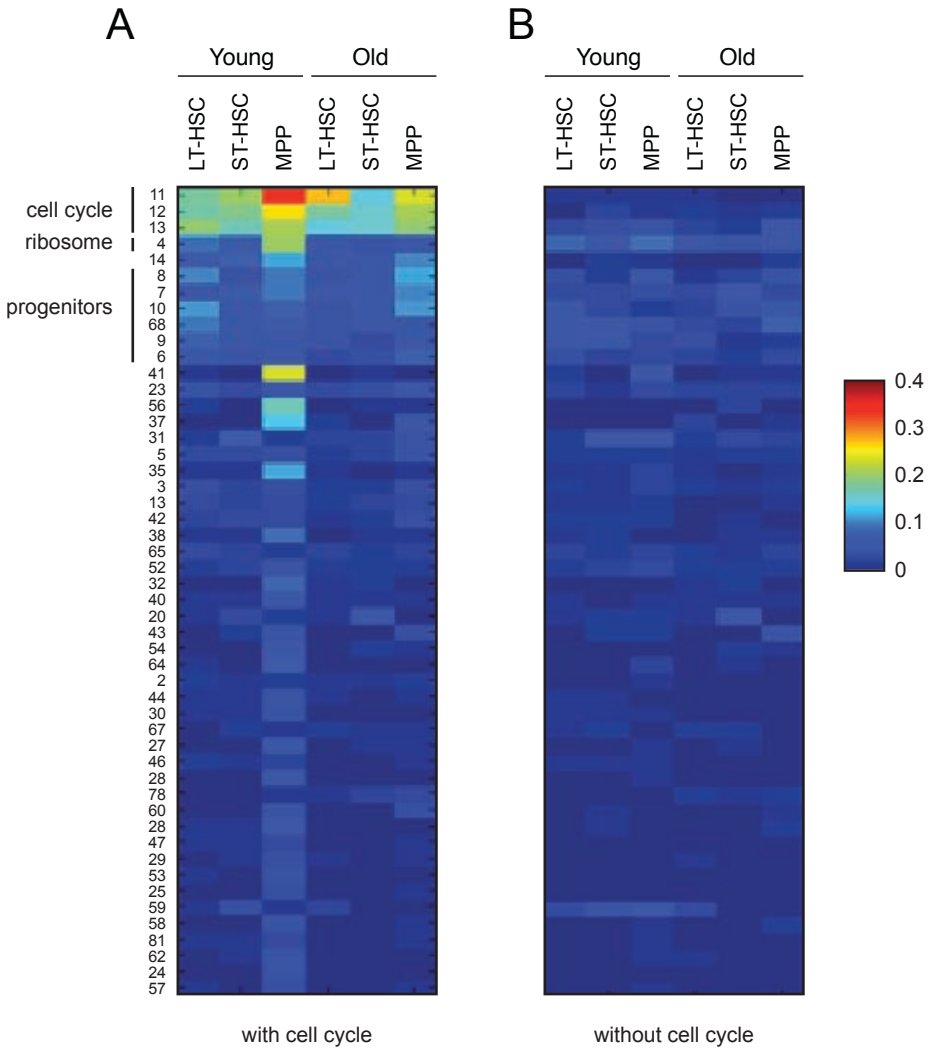

Figure S1. Coexpression of hematopoeitic transcriptional modules across single cells

(A-B) In each of the six cell populations (columns) shown is the average Pearson correlation coefficient (color bar, top) among genes from each Coarse Transcriptional Module defined by the Immunological Genome (ImmGen) Project (rows), sorted by their average coexpression, analyzed either on all cells (A) or after excluding all cycling cells (B). Module annotations are shown for some of the top modules in which annotations were defined by the ImmGen Consortium. Almost all of the highest correlations were cell cycle dependent and the strongest remaining coexpression was among ribosomal genes (module #4).

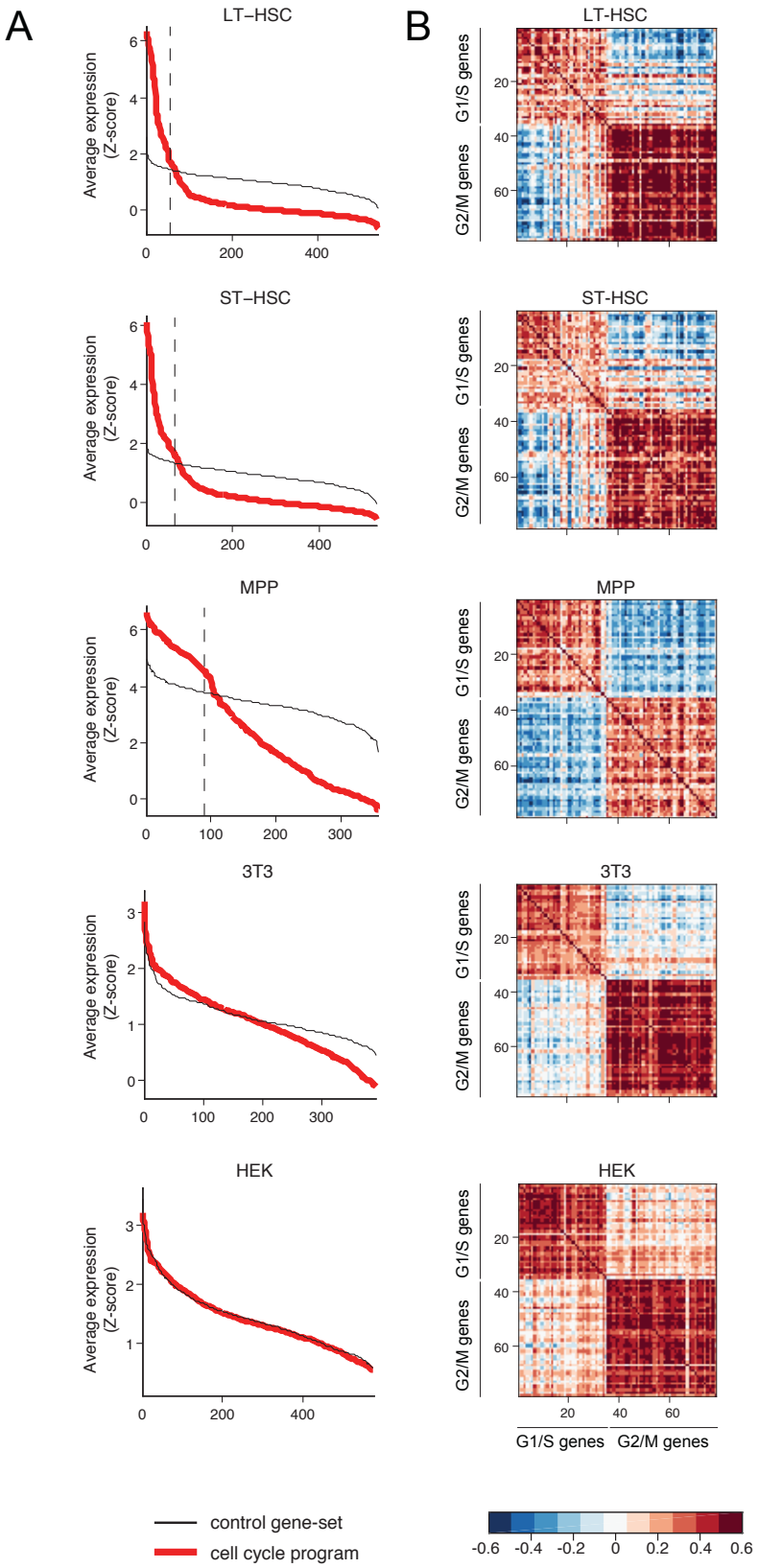

Figure S2. Meta analysis of cell cycle across 5 cell types

(A) Score of the cell cycle program (in red) defined as an average expression of G1/S and G2/M gene-sets (Z-score, *y*-axis), compared to the levels of randomly selected control gene-sets (in black) (with matched average expression level). Dashed line separates cycling (to the left of the line) and non-cycling (to the right) cells. (B) Co-expression of genes in the G1/S and in the G2/M programs among the subset of cells that were identified as cycling in (A).

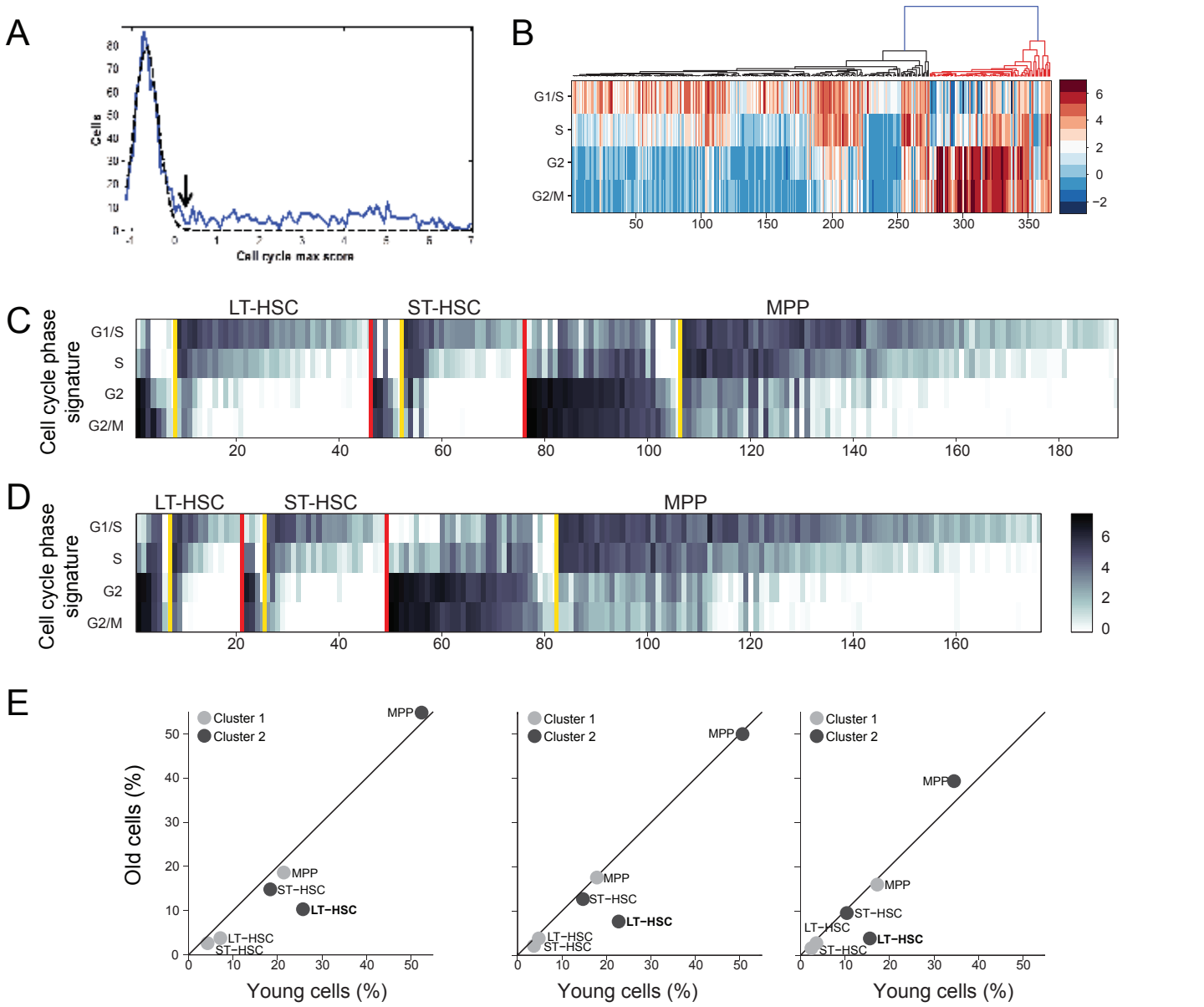

Figure S3. Clustering cells by cell cycle expression programs

(A) Signature based distinction of cycling and non-cycling cells. Shown is the distribution of the maximum cell scores (of four cell cycle signatures) (blue) and a least-squares Gaussian regression (black) performed with zero weights for all points above zero in order to fit the main peak while disregarding the long right tail. The fitted Gaussian distribution was used to define a p-value for each cell and the black arrow represents the corresponding threshold with FDR=0.05. (B) Two robust clusters of cycling cells. Shown is a dendrogram (top) generated by average-linkage hierarchical clustering of the 367 cycling cells from (A) using correlation over the four cell cycle scores (average expression (log2(TPM+1) in each cell; heatmap bottom) as a distance metric (Methods). A strong separation to two clusters is apparent that preferentially express G1/S+S genes (black portion of the dendrogram) and G2/M+M genes (red portion of the dendrogram), respectively. (C, D) Cell cycle state in different cell types and ages. Shown are the scores (greyscale bar) for each of the four cell cycle signatures (rows) in each cell type (columns; separated by red vertical lines) from either young (C) or old (D) cycling cells. Within each cell type, cells are separated by their membership of the two major clusters in (B) (separated by yellow lines). (E) The depletion of G1/S cells in old LT-HSCs is observed in the cell cycle two-cluster analysis and is robust to the threshold of identifying cycling cells. The analysis in (A) was repeated with different thresholds for classifying cells as cycling, corresponding to an FDR of 0.4, 0.05, or 10-7, followed by hierarchical clustering as in (B) and definition of two clusters (a G2/M Cluster 1 and a G1/S Cluster 2). Each graph shows percentage of cells from each cell type in each cluster in young vs. old. Three graphs represent data for three FDR thresholds (from left to right 0.4, 0.05, 10-7). Despite the wide range of thresholds, the percentage of cells in cluster 1 was almost not affected. The percentage of cells in cluster 2 was affected, but the impact of aging was qualitatively robust. The frequency of cluster 2 cells in young LT-HSCs varied from 16% to 26%, and in old LT-HSCs from 4% to 10%, and these differences between young and old were significant (P<0.01) in all cases, while none of the other aging-dependent differences were significant.

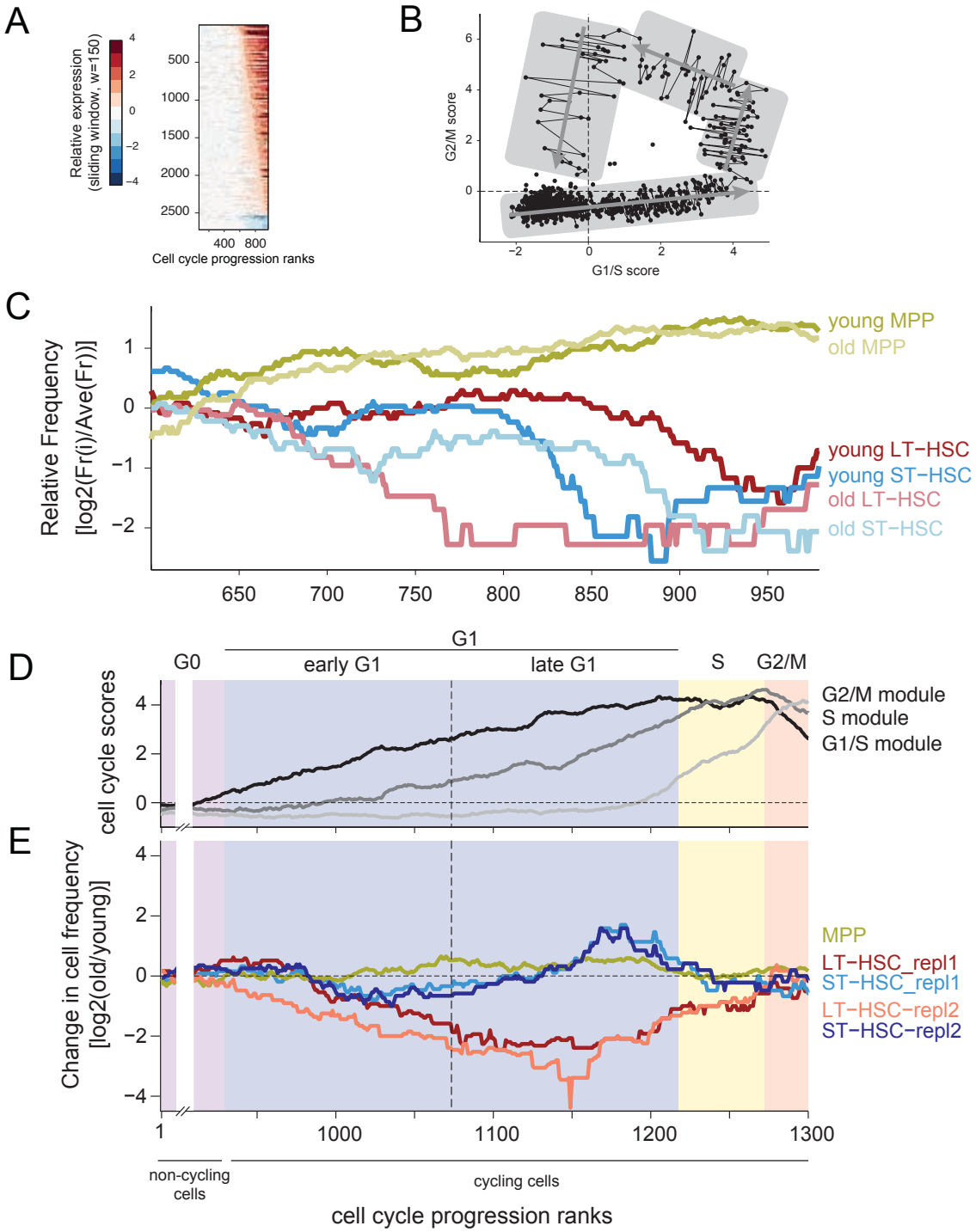

Figure S4. Ordering cells by cell cycle progression and examining changes in population frequencies
(A) A large proportion of the transcriptome is correlated with cell cycle status. Shown is the average expression of genes (rows) along the inferred cell cycle progression (columns, cells ordered according to cell cycle trajectory), as calculated with a sliding window of 150 cells, for genes with a significant upregulation (top) or downregulation (bottom) in any window of cycling cells, compared to the non-cycling cells [color bar, log2(fold change relative to G0)]. (B) Ordering cells by cell cycle progression. Shown is the same plot as in Figure 2D with edges connecting adjacent cells based on the inferred cell cycle ordering. As described in Methods, the ordering was defined by dividing the cells into four regions (marked by shaded boxes) and ordering cells within each region by the apparent direction of cell cycle progression (marked by gray arrows). Non-connected cells were not included in the cell cycle ordering due to ambiguities of their ranking. (C) The relative frequency of cells from each population (y axis; cell type and age; colored curves) along the inferred cell cycle progression (x axis), shown with a sliding window of 100 cells. Relative frequency was defined as the log2-ratio of the frequency in a specific window of cells divided by the average frequency across all windows. (D) Cell cycle progression analysis of cells and an additional biological replicate of LT-HSC and ST-HSCs. Cells were ordered according to their inferred cell cycle progression (see Figure S3A) and the average expression of G1/S, S and G2/M genes (Whitfield et al. 2002) was calculated with a sliding window of 11 cells. (E) Cell cycle distribution changes with age. For each cell type, including biological replicates of LT-HSC and ST-HSCs derived from different set of mice, shown is the log2 of the ratio between percentages of old cells divided by the percentage of young cells along the inferred cell cycle progression (with a sliding window of 150 cells). Shaded colors reflect the inferred cell cycle phases.

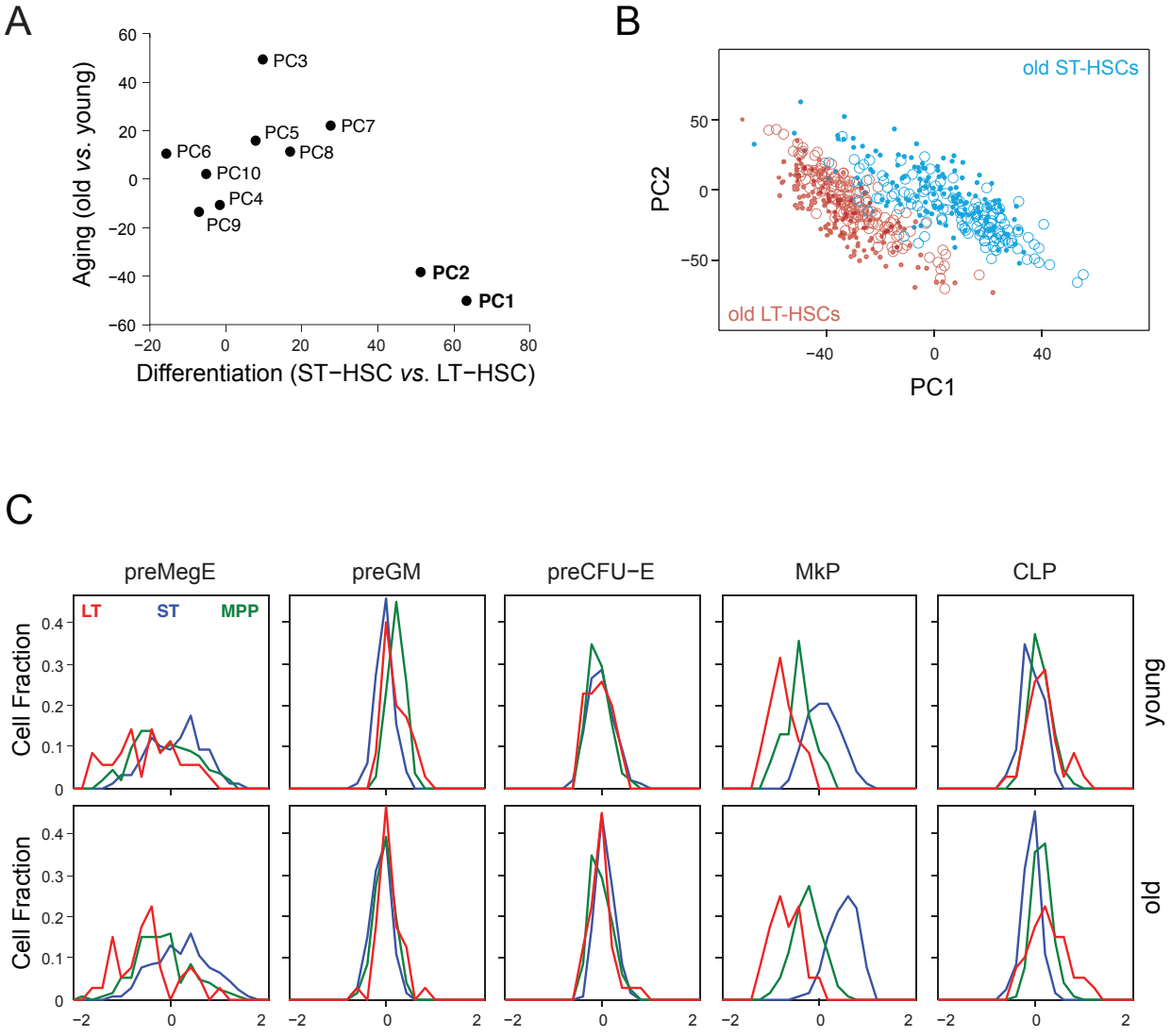

Figure S5. Differences between LT- and ST-HSCs

(**A**) Differences in the average loadings of PCs 1-10 for old vs. young HSCs (*y*-axis) and for ST- vs. LT-HSCs (*x*-axis) after excluding all cycling cells. Only the first two PCs have diametrically opposing patterns for differentiation and aging. (**B**) PCA was performed for old LT-HSCs and ST-HSCs from two biological replicates after excluding all cycling cells (replicate 1 – dots, replicate 2 – open circles). Plot shows the loadings of PC1 and PC2, colored based on their cell type and age as in Figure 3. (**C**) Distribution of the signature scores for 5 gene-sets (preMegE, preGM, preCFU-E, MkP, CLP) (Sanjuan-Pla et al. 2013) (*x*-axis) for LT-HSC (red), ST-HSC (blue) and MPP (green) in young (top) and old (bottom) mice.

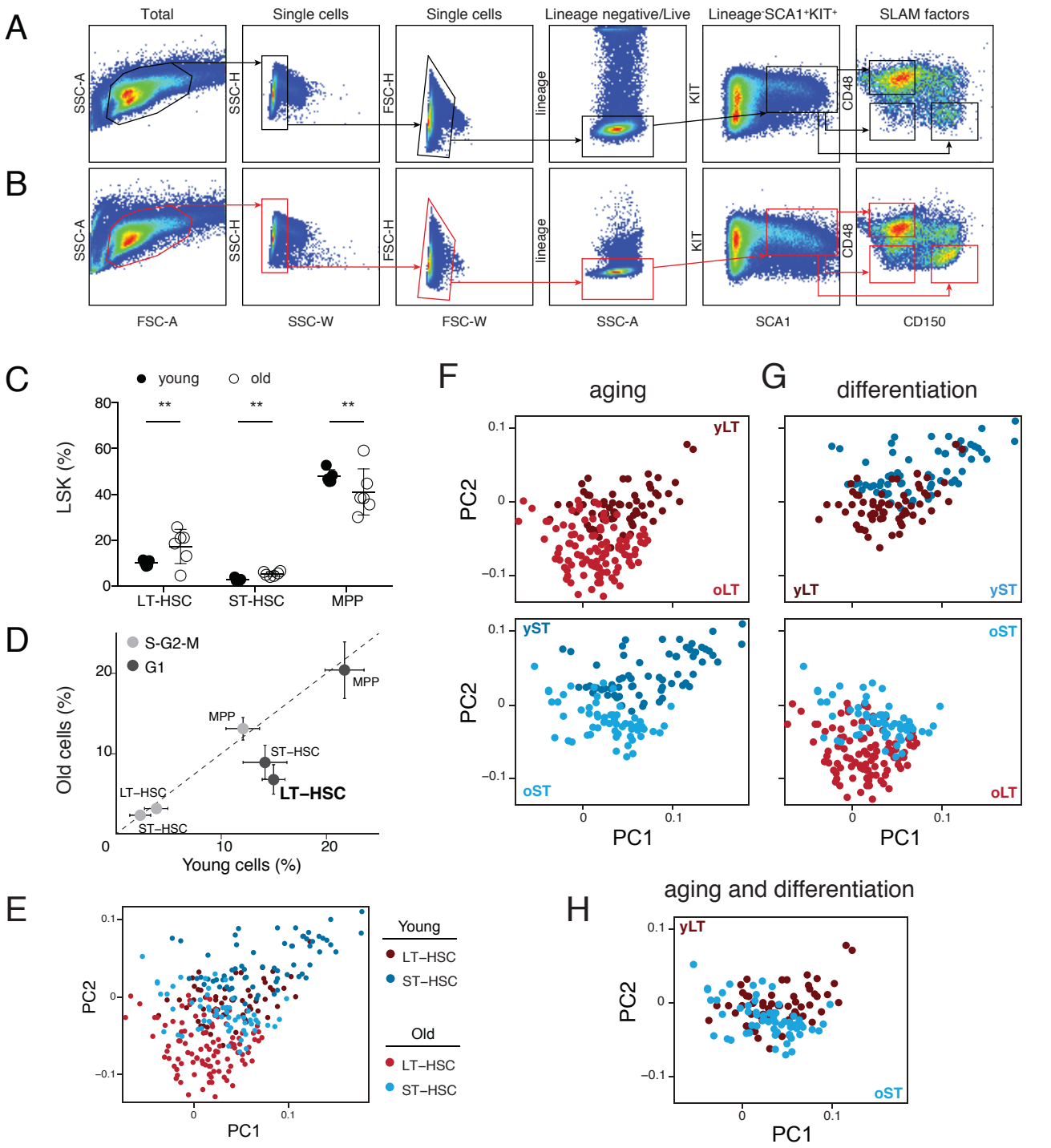

Figure S6. Age-associated changed in DBA/2

(A-B) Overview of sorting strategy for DBA/2 mice. Bone marrow cells were subjected to FACS sorting to obtain individual cells and matching populations from young (A, same plots as in Figure 6A) and old mice (B). (C) Shown are frequencies of LT-HSC, ST-HSC, and MPPs (*x*-axis) in young (black) and old (white) DBA/2 mice as percentage of stem cell compartment (lineage- Sca1+cKit+, LSK). Statistically significant differences are indicated by ** ($p<0.01$). (D) Lower frequency of G1 cells among LT-HSCs based on FACS analysis. Shown are cell frequencies in G1 (black) and S-G2-M (grey) in cells from old (*y*-axis) and young (*x*-axis) mice based on intracellular staining with Ki67/Hoechst. (E-H) HSC aging and differentiation are associated with opposite expression programs. PCA was performed for all non-cycling cells, and each of the top 2 PCs distinguish cells by their cell type and age, with higher scores for young and differentiated HSCs and lower scores for old and less-differentiated cells. Each plot shows the loadings of PC1 and PC2, colored based on their cell type and age; all six populations in (E), and the same plot is shown with only specific pairs of populations that differ by aging in (F), by differentiation in (G), and by both in (H).

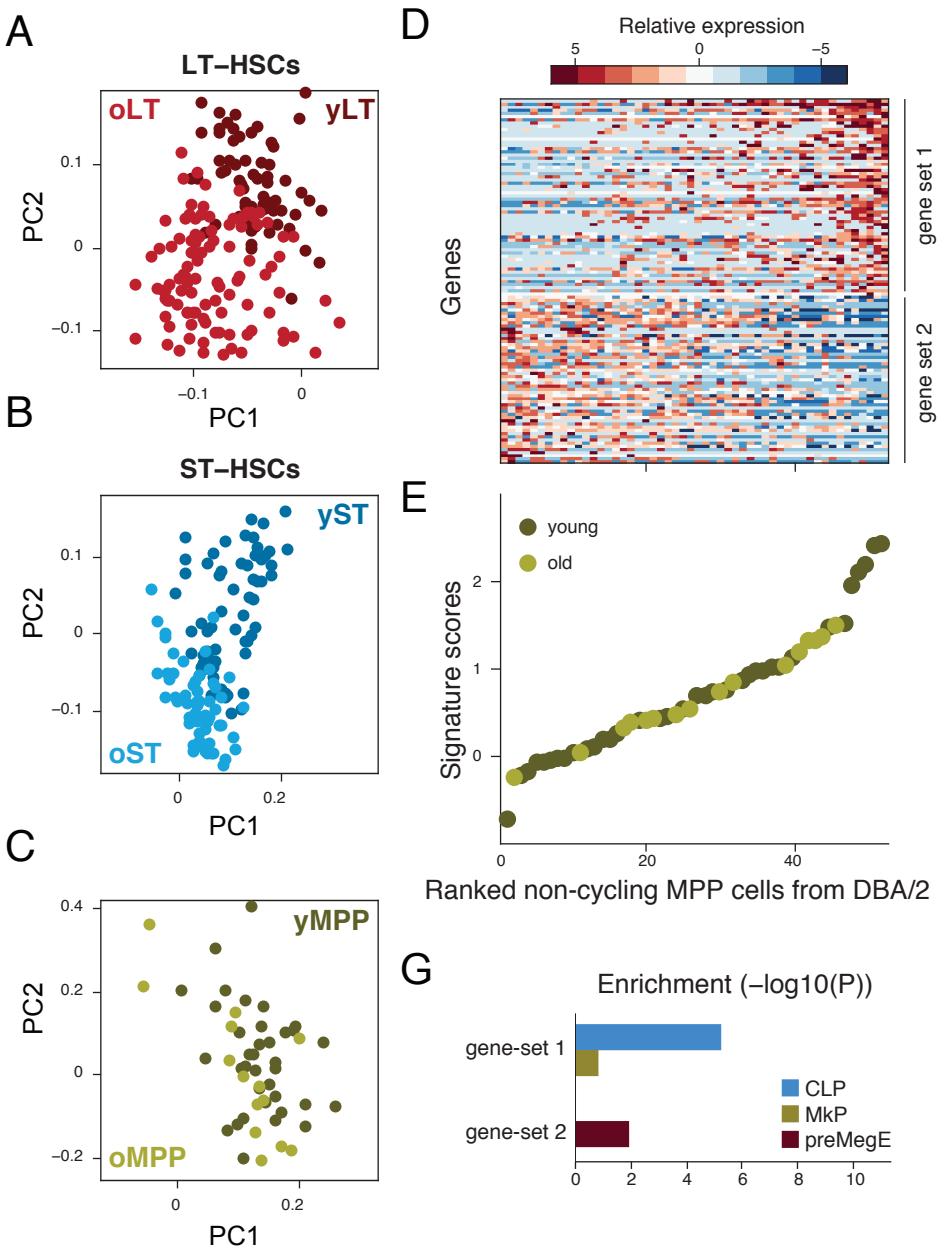

Figure S7. Subset of cells within immunophenotypically defined MPPs in DBA/2
(A-C) MPPs profiles are not distinguishable by age. PCA was performed independently for non-cycling LT-HSCs (A), ST-HSCs (B) and MPPs (C). Each plot shows the loadings of PC1 and PC2, colored based on their cell type and age. Higher scores for young HSCs and lower scores for old cells are characteristic for LT-HSCs (A) and ST-HSCs (B), but not for MPPs (C). Two distinct modules in MPPs. Heat map shows the expression of genes from two distinct gene sets (rows; gene set 1 – lymphoid-biased; and gene set 2 – myeloid-biased) across all non-cycling MPPs (columns). (E) Non-cycling MPPs from both young and old DBA/2 mice form a continuous spectrum along the two states. Shown are the signature scores (average normalized expression of gene set1 minus that of gene-set2) for each non-cycling MPP from young (dark green) or old (light green) mouse. MPPs are ranked by increasing scores (x-axis). (G) Gene set enrichment analysis based on defined progenitor sets (CLP, MkP and preMegE) within gene sets (gene set 1 and gene set 2) defining two subsets of MPPs in DBA/2.

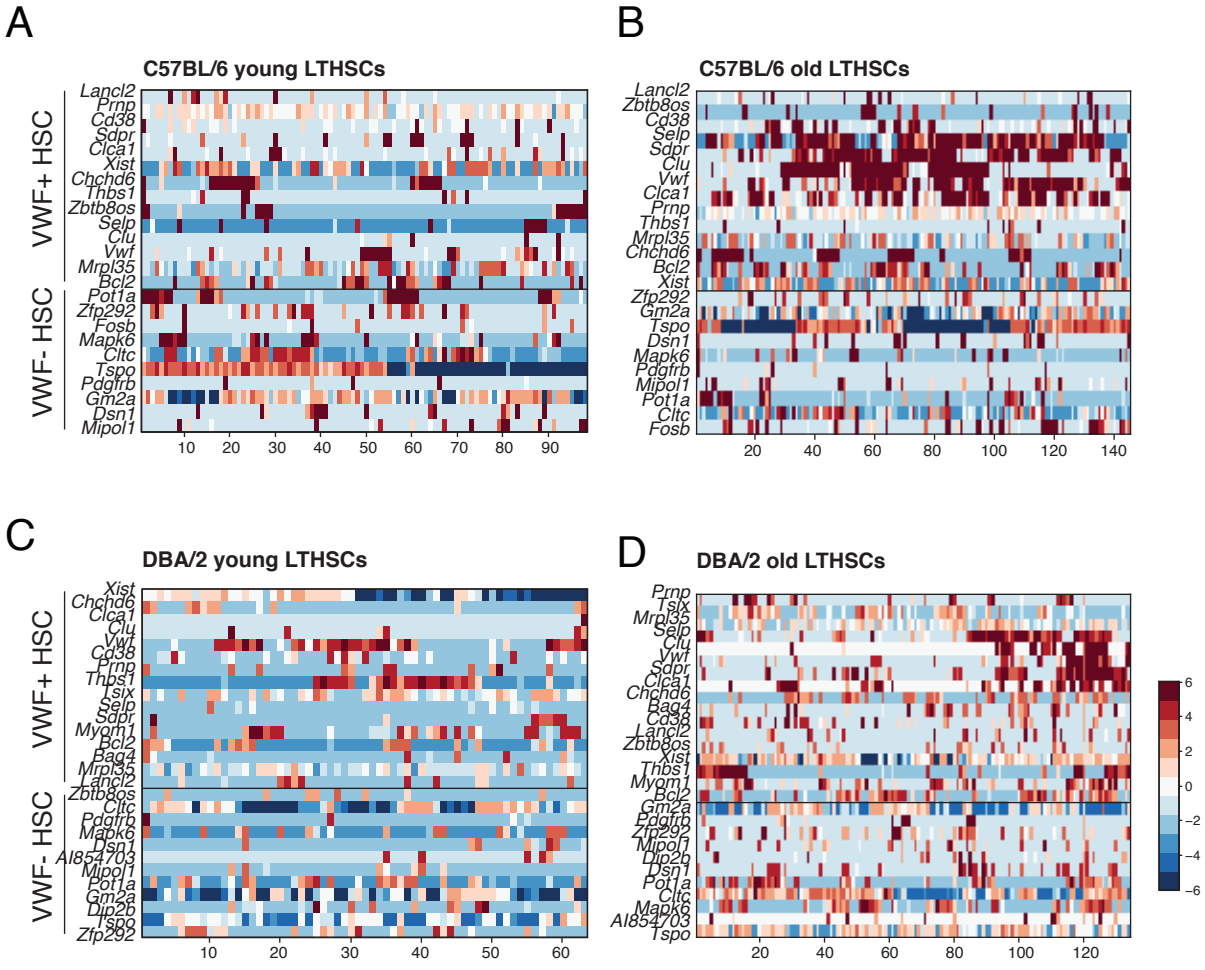

Figure S8. Lack of discernible VWF+ cells signature in LT-HSCs from young and old C57BL/6 and DBA/2 mice

(A-D) Heatmaps shows cells clustered based on previously defined signatures of VWF+ (platelet-biased LT-HSCs) and VWF- cells (Sanjuan-Pla et al. 2013) within young and old LT-HSCs from C57BL/6 and DBA/2 mouse strains.

Single cell RNA-seq reveals changes in cell cycle and differentiation programs upon aging of hematopoietic stem cells

Monika S Kowalczyk, Itay Tirosh, Dirk Heckl, et al.

Genome Res. published online October 1, 2015
Access the most recent version at doi:10.1101/gr.192237.115